# Review of the 9 January 2024 Claremont, NC Tornado

## 1. Event Overview

A powerful storm system impacted much of the region on 9 January 2024 bringing a myriad of hazards to the western Carolinas and northeast Georgia, including winter weather, flooding and severe thunderstorms. A line of thunderstorms, some of which were severe, moved across the Upstate of South Carolina during the morning hours and into the North Carolina foothills and Piedmont by early afternoon. Numerous reports of wind damage were received (Fig. 1) and one tornado was confirmed in the Claremont community in Catawba County, North Carolina (Fig. 2). A subsequent damage survey determined that a tornado touched down at 1727 UTC and tracked for nine miles from south of the city of Claremont to Interstate 40 in Iredell County just on the east side of the Catawba River. The tornado was 250 yards wide and had estimated peak winds of 110 mph. Damage was rated at EF-1 on the Enhanced Fujita Scale. Tragically, the tornado struck a mobile home community where one fatality occurred along with 4 injuries.

Unfortunately, no tornado warning was issued for this storm with the tornado also forming north of the tornado watch that was in effect (Fig. 3). The Storm Prediction Center (SPC) did have a marginal risk for severe thunderstorms across Catawba and Iredell counties (Fig. 4) with a 2% chance for a tornado within 25 miles of a point (Fig. 5). Forecaster analysis, based on available data during the event, determined that the environment over northern Catawba County was not conducive to the formation of tornadoes.

The following event review will serve to assess the synoptic and mesoscale environments along with radar data to determine how a deadly tornado was able to form in an otherwise unfavorable environment. Several hypotheses for the tornadic development will be discussed along with recommendations for future severe weather events.

## 2. Synoptic and Mesoscale Analysis

*a. Synoptic Analysis*

A strengthening, deepening low pressure system moving rapidly from the Southern Plains to the Midwest on 8-9 January set the stage for multiple significant weather threats across portions of the western Carolinas and northeast Georgia, including excessive rain, freezing precipitation, gradient wind, and severe thunderstorms. A subtropical jet streak of greater than 150 kt analyzed at 250 mb moving around the base of a meridional upper trough from 1200 UTC 8 January to 1200 UTC 9 January contributed to the deepening of a closed low at 500 mb, from 534 dam centered over New Mexico at 1200 UTC 8 January, to 525 dam centered over the Ozark Plateau region by 1200 UTC 9 January (Fig. 6). After that time, the closed low would continue eastward toward the Illinois/Indiana border by 0000 UTC on 10 January. Similar deepening of the low was seen at 700 mb and 850 mb during this time period, with the low centered over Missouri at 1200 UTC on 9 January (Fig. 7). The mean geopotential height values associated with the low and trough axis were more than four standard deviations below normal at 500 mb, 700 mb, and 850 mb on the North American Ensemble Forecast System (NAEFS) initialization at 1200 UTC on 9 January (Fig. 8). The effect on the wind field across parts of the Southeast into the Carolinas, in the southeastern quadrant of the low, was dramatic.

At 1200 UTC 9 January, the upper air observation taken at Greensboro, North Carolina (Fig. 9), well to the east and ahead of the core of the stronger low-level winds, already showed a southeast wind of 40 kt at the mixed-layer lifted condensation level (MLLCL; 429 m above ground level [AGL]) and a southerly wind of 55 kt at 1000 m AGL (approximately 850 mb). The low-level wind field would only increase with time. The movement of the low was expected to draw a very strong southerly low-level jet streak of 75 kt or greater at 850 mb eastward across the western half of Carolinas between 1200 UTC and 1800 UTC on 9 January. The NAEFS 6-hour forecast valid at 1800 UTC on 9 January showed a standardized anomaly of four standard deviations above normal for the wind speed at 850 mb over the Carolinas east of the Blue Ridge, with the maximum centered near Charlotte, North Carolina (Fig. 10). The wind anomaly at 700 mb was on the order of three standard deviations above normal. The very strong low-level jet was the primary driver of the gradient wind threat across the mountains, and greatly enhanced the low-level wind shear that was the main factor in the severe thunderstorm risk. Furthermore, the low-level jet was responsible for transporting copious amounts of moisture northward from the eastern Gulf of America, which

was a primary ingredient for the excessive rainfall/flash flood threat. The NAEFS 6-hour forecast of mean precipitable water showed a positive anomaly of three standard deviations over the Carolinas east of the Blue Ridge, while the mean integrated water vapor transport anomaly was greater than 8 standard deviations above normal in a plume from north Florida to the western Piedmont of North Carolina (Fig. 11).

At the surface, the antecedent air mass across the western Carolinas was dominated by cold and dry surface high pressure with a 1030 mb center analyzed over south central North Carolina at 1200 UTC on 8 January (Fig. 12). Observations of dewpoint were in the mid to upper 20s °F with northeast wind maintaining a supply of dry air into the region. By 0000 UTC on 9 January, the progressive weather pattern moved the center of high pressure off the Delmarva Coast, which allowed surface winds to veer to easterly (Fig. 13). A mature mid-latitude cyclone of 988 mb was centered over Missouri and the mid-Mississippi River Valley region at 1200 UTC on 9 January, with another open wave of low pressure (997 mb) located over east central Alabama, while a retreating 1031 mb surface high was located off the southern New England Coast (Fig. 14). A warm/coastal front was analyzed from the Alabama low, across central Georgia, to the Coastal Plain of the Carolinas. By 1500 UTC, the latter surface low had moved over north Georgia in the vicinity of the Atlanta metro area and the warm front had lifted north along a line from near Athens, Georgia, to Charlotte, North Carolina (Fig. 15). The intense low-level flow previously noted, with a moisture source region over the Gulf of America, rapidly advected low- to mid-60s °F dew points across the warm sector over central/southern Georgia and the Midlands and Coastal Plain of South Carolina.

*b. Mesoscale Analysis*

The environment was much more complex across the Upstate of South Carolina and foothills of North Carolina to the north of the warm front. Strong deep-layer lift interacting with anomalous moisture transport (Fig. 16) fostered a persistent swath of warm advection showers during the early morning hours on 9 January that lasted until the arrival of the convective line of interest along an advancing cold front. Precipitation falling into the dry boundary layer north of the warm front, generally along and north of Interstate 85, evaporatively cooled the air mass and initiated the development of cold air damming (CAD). This event was of the in-situ classification where surface high pressure had shifted offshore and was

unable to provide significant synoptic support to damming, but had since previously passed the region leaving in place dry air at low-levels (Bailey et al. 2003). The presence of a CAD wedge created a very sharp temperature and moisture gradient across the warm front that separated the cool and stable CAD air and the open warm sector (Fig. 15).

Forecasting the demise of the CAD wedge and when it will erode is notoriously difficult, with numerical models typically having a systematic bias towards premature erosion. The evolution of the CAD wedge has major implications for where severe weather may occur. Lackmann and Stanton (2004) identified several CAD erosion processes, two of which were notable during this event. First, the intense 70-80 kt low-level jet above the CAD dome resulted in increasing shear across the inversion layer. Along the edges of the CAD dome, the shear was likely sufficiently large to result in entrainment and mixing, enhancing erosion of the CAD dome. Second, pressure falls north of the CAD dome with the approach of the deepening surface low enhanced divergence within the CAD dome allowing further northward progression of the warm front. Thus, the warm front slowly moved north through the morning hours as the in-situ CAD wedge gradually eroded in the absence of a reinforcing surface high to serve as a source of cold and dry air needed to maintain the CAD.

Regional hourly surface observations from 1400 UTC through 1700 UTC (Fig. 17) showed the warm front moving across the Charlotte area and located between Hickory, North Carolina, and Statesville, North Carolina, at 1700 UTC, 20 minutes before the tornado impacted the area. The 1700 UTC METAR observation at Hickory had an air temperature and dewpoint temperature of 40° F, while Statesville observed an air temperature and dewpoint of 55° F. Thus, one can infer that the warm front was located somewhere between the two observation sites. For the purposes of this event review, archived data from two personal weather stations located near the tornado were analyzed via WeatherUnderground. An AcuRite 5-in-1 Weather Station (temperature accuracy of +/- 2° F) located in Claremont, and a Davis Vantage Vue weather station (temperature accuracy of +/- 1° F) located just south of the town of Catawba, North Carolina, were used to further refine the location of the warm front. While the exact siting of these personal weather stations is unknown, the observations were deemed to be sufficiently reliable to assess the location of the warm front. Observations from the Claremont weather station depicted this location to be on the cool and stable side of the warm front,

with northeast winds and temperature and dewpoint in the upper 40s °F (Table 1). The weather station near Catawba, on the other hand, was on the warm side of the front with the warm frontal passage noted between 1630 - 1635 UTC, with winds shifting to southeast and temperature and dewpoint rising into the mid 50s °F (Table 2). Based on these data, it can be inferred that the warm front was more precisely located between Claremont and Catawba. The tornado track, when overlaid on a map showing the location of the personal weather stations, suggested the tornado occurred either right along or just barely south of the warm front (Fig. 18).

The previously discussed intense winds at 850 mb and 700 mb fostered highly anomalous values of low- and deep-layer vertical wind shear that met or exceeded daily maximum values based on sounding climatology at Greensboro. Archived data from SPC's Rapid Refresh (RAP)-based surface objective analysis were retrieved at 1700 UTC, just prior to the tornado. Surface-to-1 km bulk wind shear values were around 60 kts (Fig. 19) with around 900 $m^2 s^{-2}$ of surface-to-1 km storm relative helicity (SRH; Fig. 20) and around 1300 $m^2 s^{-2}$ of surface-to-3 km SRH (Fig. 21). Deep-layer shear was equally extreme with around 90 kts of surface-to-6 km bulk shear (Fig. 22). Instability was very weak, as positive surface-based convective available potential energy (SBCAPE) struggled to make northward progress, with the 100 J $kg^{-1}$ isopleth analyzed near Columbia, South Carolina (Fig. 23). The 100 J $kg^{-1}$ isopleth for 100 mb mixed-layer CAPE (MLCAPE) was slightly farther north, but still well south of Catawba County (Fig. 24).

Also available during the event was near real time temperature, dewpoint and wind data collected by commercial aircraft ascending and descending at Charlotte Douglas International Airport (KCLT). Data were transmitted through the Aircraft Communication Addressing and Reporting System (ACARS) and plotted on a traditional Skew-T Log-P sounding. The 1720 UTC KCLT ACARS sounding (Fig. 25) was heavily utilized by forecasters during the event. The sounding supported the SPC RAP-based wind shear analysis with 87 kts of surface-to-6 km bulk wind shear and 58 kts of surface-to-1 km bulk shear. The thermodynamic profile also depicted a deep isothermal layer extending from the surface to just above 850 mb where a notable inversion was in place (-465 J $kg^{-1}$ of mixed-layer convective inhibition (MLCIN)) with elevated instability (370 J $kg^{-1}$ of most unstable CAPE (MUCAPE)) rooted above the inversion layer. Of note,

though, is that 70 J $kg^{-1}$ of SBCAPE was sampled within the predominantly isothermal layer. The KCLT METAR at 1718 UTC had a temperature of 60° F and a dewpoint of 57° F, which were 5° F warmer and 2° F higher, respectively than the Catawba personal weather station. Thus, it can be inferred that any SBCAPE extending farther north into Catawba County was likely less than the 70 J $kg^{-1}$ noted on the KCLT ACARS sounding.

Such environments are commonly characterized as high-shear, low-CAPE (HSLC), which are frequently found during the cool season in the southeast United States (Sherburn and Parker 2014). HSLC environments are a challenge for operational meteorologists as conventional techniques for forecasting significant severe weather typically perform poorly (Guyer and Dean 2010), and severe weather can occur with little to no cloud-to-ground lightning (McAvoy et al. 2000). Furthermore, forecasting parameters that include CAPE as a constituent, such as the significant tornado parameter (STP), struggle to adequately represent the severe weather risk in HSLC environments (Sherburn et al. 2016). The Claremont Tornado event is no exception, with the STP providing little support with non-zero values confined well south of the area (Fig. 26). HSLC environments are traditionally characterized by SBCAPE less than 500 J $kg^{-1}$ and surface-to-6 km bulk shear greater than 35 kts (Sherburn and Parker 2014). This event is a significant outlier compared to established HSLC climatology with highly anomalous shear and minuscule CAPE.

## 3. Radar Analysis

Three different radars were used to interrogate convection during the event: the Weather Surveillance Radar - 88 Doppler at the NWS office in Greer, South Carolina (the KGSP radar), the Climavision radar in southeast Lincoln County, North Carolina (the V025 radar, used as part of an evaluation agreement between Climavision and the NWS), and the FAA Terminal Doppler Weather Radar on the northwest side of Charlotte (the TCLT radar), which had the best viewing angle (Fig. 27). A quasi-linear convective system (QLCS) was moving across the Upstate of South Carolina as early as 1600 UTC with the QLCS approaching KGSP at 1613 UTC (Fig. 28). As the QLCS passed over KGSP, the radar sampled base velocity values of 50 kts at 56 ft Above Radar Level (ARL) at 1611 UTC (Fig. 29). However, the KGSP METAR indicated that the cold and stable CAD airmass was still in place at that location with a temperature of 41° F and a dewpoint of 39° F. As such, the QLCS was elevated above the CAD

inversion with little of this wind able to penetrate into the shallow stable layer below the CAD inversion. This was confirmed by the KGSP ASOS with a peak wind gust of only 25 kts as the QLCS moved through. The QLCS subsequently propagated northeast with the northern extent of the QLCS reaching into the North Carolina foothills. The QLCS was approaching the southwest corner of Catawba County at 1701 UTC (Fig. 30) with a very narrow and shallow structure. No 50 dBZ echoes extended to 10000 ft ARL with very little structure of the line visible on the KGSP 1.8° elevation angle at roughly 11000 ft ARL (Fig. 31). Furthermore, surface observations at 1700 UTC (Fig. 17) continued to indicate that the QLCS was elevated above the CAD inversion layer. Isolated reports of fallen trees were received west (upstream) of Catawba County, but this was attributed to a combination of non-thunderstorm sub-severe wind gusts and saturated soils from persistent rains ahead of the QLCS.

As the QLCS moved into Catawba County, TCLT obtained a better viewing angle as the distance from KGSP further increased. This was key for anticipating tornadoes, and especially QLCS tornadoes, due to the shallow nature of the formation mechanisms (Lovell and Parker 2022). Using TCLT allowed for viewing the lower levels of the atmosphere down to 700-800 ft ARL compared to KGSP which could only sample down to approximately 5000 ft ARL on the lowest (0.2°) elevation angle above Catawba County. At 1722 UTC, five minutes prior to tornadogenesis, TCLT continued to depict poor reflectivity structure with a narrow and shallow QLCS (Fig. 32). More intriguing, however, was the velocity data showing broad cyclonic convergence over south central Catawba County (Fig. 33). Three minutes later, at 1725 UTC (two minutes before tornadogenesis), the area of cyclonic convergence began to tighten northeast of Maiden with a more defined signature present (Fig. 34). By 1727 UTC, at the time the tornado touched down, a cyclonic convergence signature persisted south of Claremont, but a tighter velocity couplet indicative of a possible tornado was not yet present (Fig. 35). While noisy, a more notable velocity couplet was apparent at 1729 UTC as the tornado was ongoing (Fig. 36). This signature persisted for two minutes on the 1730 UTC and 1731 UTC volume scans (Figs. 37 and 38) before the QLCS moved into an area of static beam blockage extending along the Catawba and Iredell county border. The tornado dissipated while the storm was in the beam blocked area.

For comparison purposes, the data from KGSP at 1724 UTC have been provided (Fig. 39). Due to intense background environmental winds, storm-relative velocity (SRV) was used with a storm motion from 221° at 64 kts. Convergence was noted along the leading edge of the QLCS, but no cyclonic rotation was apparent. It was not until 1731 UTC at a height of 5000 ft ARL that evidence of a possible rotation signature became evident between Claremont and Catawba (Fig. 40). This signature persisted for one more volume scan before dissipating. The closest radar in the vicinity of the reported tornado was a Climavision system, V025. However, there was no operationally useful data due to attenuation of the beam caused by moderate rain ahead of the QLCS. The Climavision radars operate at X-band frequencies, 3 cm wavelength, unlike the KGSP WSR-88D that operates at S-band with a 10 cm wavelength. This allows the shorter wavelength Climavision radar to obtain much greater spatial resolution compared to the WSR-88Ds; however, 3 cm X-band radars suffer from significant attenuation in rain (Park et al. 2005). Resulting attenuation from persistent moderate rain limited the sampling ability of the Climavision radar, drastically reducing the range at which it could properly sample the QLCS. There was one volume scan from V025 at 1725 UTC that resolved broad cyclonic convergence northeast of Maiden, NC (Fig. 41), but significant attenuation thereafter limited the range of the radar, especially as the heavier rain associated with the QLCS moved over the radar, with no additional features of the tornadic portion of the line sampled. The authors note that Climavision is exploring new processing approaches to reduce the impacts of signal attenuation inherent with X-band radar data when precipitation is occurring at the radar location.

## 4. Discussion

A strongly forced QLCS moved within a HSLC environment across the foothills and western Piedmont of North Carolina. However, the northern extent of surface-based instability was in question. Real-time analysis determined that the environment over northern Catawba County was not favorable for tornadoes owing to the lack of SBCAPE and poor thermodynamic profiles noted on the KCLT ACARS sounding. Furthermore, poor reflectivity structure of the QLCS and a lack of wind damage reports contributed to the warning decision process, and eventually the decision to not issue a tornado warning.

The tornadogenesis process for QLCS tornadoes and how the environment is related to said process, radar signatures commonly associated with QLCS tornadoes, and how these factors played into the warning decision process on 9 January 2024 are discussed in the following section. Several hypotheses are also presented for how tornadic development was able to occur in a seemingly unfavorable thermodynamic environment.

*a. QLCS Tornadogenesis Process and Role of the Environment, Radar Signatures Associated with QLCS Tornadoes, and the Warning Decision Process*

It is important for forecasters to understand the QLCS tornadogenesis process and what role the environment plays, especially in terms of instability. One conceptual model that receives considerable operational attention is discussed by Schaumann and Przybylinski (2012). Within this model, previous work has shown that line-embedded mesovortices are responsible for the production of QLCS tornadoes (Przybylinski et al. 2000) with tornadogenesis emanating from mesovortices occurring rapidly with a mean lead time of approximately five minutes (Trapp et al. 1999). The genesis of mesovortices is linked to the tilting and stretching of horizontal vorticity within the updraft/downdraft convergence zone (UDCZ) where deep and upright updrafts are produced by a balance of low-level shear and cold pool generated horizontal vorticity, which in turn act to maximize vortex stretching (Schaumann and Przybylinski 2012). While frequently used in the National Weather Service, this is just one conceptual model for QLCS tornadogenesis, however, and does not cover all observed QLCS tornadoes. Additional research and field projects are ongoing in an attempt to better understand the QLCS tornadogenesis process with a recent multi-year project (PERiLS - Propagation, Evolution, and Rotation in Linear Storms) focused on this very topic (Kosiba et al. 2024).

Instability, particularly low-level instability in the surface-to-3 km layer (3CAPE), also plays an important role in the tornadogenesis process with a direct relationship between CAPE and maximum updraft strength ($W_{max}$):

$$W_{max} = \sqrt{2(CAPE)}$$

Greater values of CAPE, and especially 3CAPE, would support a stronger updraft and enhanced stretching of vorticity and subsequent

tornadogenesis. Hampshire et al. (2018) further expands on the low-level CAPE and tornado relationship, showing a statistically significant positive correlation between 3CAPE and tornado intensity.

The environment during the Claremont Tornado was assessed to have more than sufficient low- and deep-layer vertical wind shear for storm organization and the development of streamwise horizontal vorticity. The main uncertainty was whether there was sufficient buoyancy for deep updrafts to tilt and stretch the vorticity and yield tornadogenesis. The SPC mesoanalysis did not indicate the presence of SBCAPE across Catawba County, however this dataset can be prone to error in low-CAPE environments, especially in heterogeneous and rapidly evolving environments (Coleman et al. 2018). The KCLT ACARS sounding provided a better depiction of the actual environment with reliable near-real time data. ACARS temperature data have been found to have a root mean square error of only 1 K (1.8° F) (Benjamin et al. 1999) with the 1720 UTC KCLT sounding (Fig. 25) also comparable to observations from the KCLT ASOS. Thus, the ACARS data can be reliably used to assess the near-storm environment, keeping in mind that the airport was located 33 miles southeast of the tornado and the sampling profile was governed by the approach and departure procedures in use at the time. As previously noted, 70 J $kg^{-1}$ of SBCAPE was sampled on the 1720 UTC ACARS within a very shallow and weakly unstable surface layer. Very close inspection of the ACARS sounding reveals an extremely shallow (surface to 500 m, or less) layer where the 70 J $kg^{-1}$ of SBCAPE was located before the temperature profile became isothermal and eventually encountered an inversion layer rooted just above 850 mb. While some degree of SBCAPE may have extended into Catawba County, it was likely less than the 70 J $kg^{-1}$ observed on the ACARS sounding. Furthermore, forecaster analysis during the event determined that the isothermal temperature profile and capping inversion would be detrimental to buoyancy and deep updrafts needed to effectively stretch vorticity within line embedded mesovortices and produce tornadoes.

Radar signatures also play a prominent role in the warning decision process in addition to having a proper conceptual model for QLCS tornadogenesis and understanding of the mesoscale environment. Previous work has identified a number of reflectivity signatures commonly associated with QLCS tornadoes (McAvoy et al. 2000, Lane and Moore 2006, and Davis and Parker 2014). Schaumann and Przybylinski (2012)

combined several of these signatures with the previously discussed physical mesovortex genesis mechanisms to develop a “Three Ingredients Method” for anticipating QLCS mesovortices and associated tornadoes. The method requires the following three ingredients to be coexisting:

1. A portion of a QLCS in which the system cold pool and ambient low-level shear are nearly balanced or slightly shear dominant.
2. Where surface-to-3 km line-normal bulk shear magnitudes are equal or greater than 30 kts.
3. Where a rear inflow jet (RIJ) or enhanced outflow causes a surge or bow in the line.

The NWS Central Region Tornado Warning Improvement Project further expanded this work to include the Three Ingredients Method as part of a more robust four step QLCS Mesovortex Warning System with the steps as follows:

1. Use the Three Ingredients Method to anticipate areas where mesovortex genesis is likely over the next 30-45 minutes.
2. Identify the presence of confidence-building radar signatures/environmental parameters and nudgers that are indicative of increased likelihood for tornadoes.
3. Determine the number and quality of confidence builders and nudgers to issue heightened warning products.
4. Draw an effective warning polygon to capture motion and evolution of key features over the next 30-45 minutes.

This four step QLCS Mesovortex Warning System was in use during the Claremont Tornado. Figures 42 through 45 show the QLCS Mesovortex Warning System reference sheets used by NWS forecasters with examples of the Three Ingredients Method along with common radar signatures and environmental parameters associated with QLCS tornadoes (confidence builders and nudgers). For the Claremont Tornado, starting with the Three Ingredients Method, the cold pool of the portion of the QLCS moving northeast into Catawba County was balanced with the ambient low-level shear (Figs. 32 and 33). The surface-to-3 km line-normal bulk shear was well in excess of the 30 kt requirement. A descending RIJ or surge/bow in the line was not apparent, however, satisfying only two of the three necessary ingredients. For confidence builders and nudgers, poor reflectivity structure of the line made it very

difficult to assess whether any were present, but an argument can be made that a subtle surge may have occurred along the portion of the line that produced the tornado. Whether at least 40 J $kg^{-1}$ of 3CAPE extended that far north was indeterminate, which resulted in possibly just one confidence builder. A tighter velocity couplet was eventually apparent (Fig. 37), but it was after the tornado was already ongoing, and thus not included as part of the QLCS mesovortex warning process which is intended to anticipate QLCS tornadoes prior to their formation.

Forecasters incorporated both the mesoscale environment and radar signatures into their analysis and warning decision process during the event. The decision not to issue a tornado warning for the QLCS was ultimately based on the dearth of instability needed to stretch low-level vorticity, poor thermodynamic profiles sampled in the KCLT ACARS sounding, not meeting all requirements for the Three Ingredients Method, insufficient confidence builders and nudgers as part of the QLCS Mesovortex Warning System and generally poor reflectivity structure of the very narrow and shallow QLCS. Furthermore, storm motions were exceptionally fast (64 kts) with the tornadogenesis process happening rapidly in a matter of five minutes or less, leaving forecasters with very little time to quickly assess an extremely challenging warning environment. The QLCS also extended through southern portions of the County Warning Area, forcing forecasters to interrogate numerous other segments of the line in addition to the portion that produced the Claremont Tornado.

*b. Hypotheses for Tornadic Development*

It is imperative to investigate how a tornado is able to develop in what appears to be an unfavorable environment for tornadogenesis. Understanding what allowed this tornado to form will help forecasters better anticipate such low predictability events in the future. The Claremont Tornado appears to have been governed by subtle mesoscale and storm-scale features. Identifying these features and how they support tornadogenesis will help refine the conceptual model for anticipating QLCS tornadoes. The authors hypothesize that a combination of relatively small mesoscale changes in the environment not captured by available model guidance or the SPC RAP-based mesoanalysis, influence from the nearby warm front, local storm-scale processes, and the release of horizontal shearing instability (HSI) all contributed to the tornadogenesis process. The following subsections will discuss each of these factors in

greater detail. It is important to note that these are just hypotheses and limited near-storm observational data prevents knowing exactly how the tornado was able to develop.

*(i) Subtle Changes in the Mesoscale Environment and Local Storm-Scale Processes*

The KCLT ACARS sounding was heavily referenced during the event and was the most accurate depiction of the atmospheric profile available. Thus, it will be used as the starting point and primary reference for how small mesoscale environmental changes and local storm-scale processes may have influenced the thermodynamic profile and available instability. There are several mechanisms that would increase instability in the ACARS sounding which include warming of the surface, increasing the surface dewpoint, and lifting/cooling of the temperature inversion rooted just above 850 mb. There was little to no surface warming owing to persistent moderate rain ahead of the QLCS, so any increase in CAPE would have been driven by an increase in surface dewpoint and/or removal of the temperature inversion through local storm-scale processes. Coleman et al. (2018) and King et al. (2017) both demonstrate how the environment can rapidly evolve on the mesoscale with notable increases in CAPE, which is poorly captured by SPC's mesoanalysis and most short-term high-resolution model guidance. While large changes in the environment did not occur during this event, there were subtle differences between the SPC mesoanalysis, model guidance, and the observed environment that likely contributed to a subtle unexpected increase in low-level buoyancy. Based on the ACARS thermodynamic profile, it would appear as if any SBCAPE that was present at the time of the Claremont Tornado would have been focused in the low-levels which has been shown to support robust convection in weak CAPE environments (McCaul and Weisman 2001). However, elevated MUCAPE above the temperature inversion cannot be ignored. Storm-scale processes may have proven sufficient to locally erode the temperature inversion and allow the QLCS to tap into more favorable thermodynamic profiles aloft, thus yielding more instability than anticipated.

The experimental Warn-on-Forecast System (WoFS, Heinselman et al. 2023), a rapidly-updating, high-resolution ensemble model system designed by the National Severe Storms Laboratory (NSSL) to provide continuous, probabilistic predictions of hazards in individual thunderstorms

out to six hours, was run during the event with a domain centered over the Carolinas. The first run was initialized at 1700 UTC with the first data arriving to the web viewer at 1720 UTC, so unfortunately it was not available for forecasters to evaluate in advance of the Claremont Tornado (P. Burke, NOAA/NSSL, 2024, personal communication). However, the data were archived and proved useful in helping to compare the subtle differences between the modeled environment and actual surface observations. From the start, WoFS initialized temperatures too cool in the warm sector (Fig. 46) with dewpoints also too low (Fig. 47). By 1800 UTC, WoFS dewpoints continued to run too low compared to observations with indications of a narrow area of higher dewpoints extending from Charlotte into southeast Catawba County (Fig. 48). This narrow moisture axis was even more apparent in surface theta-e fields with a theta-e ridge extending from the western side of Charlotte into central Catawba County at 1725 UTC (Fig. 49). A WoFS forecast sounding 12 miles southeast of the tornado valid at 1715 UTC (Fig. 50) depicted a similar thermodynamic profile to the ACARS soundings with an isothermal layer extending to a capping inversion at 850 mb. A key difference, however, was that the WoFS sounding did not depict any SBCAPE confined to a shallow weakly unstable layer as sampled in the ACARS sounding. This also had major implications on the vertical location of the effective inflow layer with the WoFS effective inflow layer elevated above the temperature inversion, whereas the ACARS sounding had a very shallow surface-based effective inflow layer where the limited SBCAPE was confined. Similar to the SPC mesoanalysis, WoFS also underestimated the northward extent of a narrow tongue of moisture and its contributions to instability.

*(ii) Warm Frontal Influence and Synoptic Contributions*

In addition, the very close proximity of the warm front to the tornado track likely played a key role in enhancing the near-storm environment to be more favorable for tornadogenesis. Coleman et al. (2018) also discussed the influence of a thermal boundary on a significant tornado that occurred in central Alabama in what was initially assessed to be an environment that was not conducive for tornadoes based on traditional mesoanalysis. Surface observations at 1700 UTC (Fig. 17) indicated a very sharp temperature and dewpoint gradient across the warm front separating the cold stable CAD wedge and the open warm sector. This sharp thermal and moisture boundary fostered a band of strong frontogenesis extending along the warm front (Fig. 51). The resulting frontogenetical circulation

produced upward motion and associated horizontal convergence on the warm side of the front, subsequently leading to a deepening of the moist layer with a local maximum in surface dewpoints along the boundary. The thermally direct circulation of a warm front has also been shown to increase vertical wind shear in the front-normal direction (Coleman et al. 2018), although the shear magnitude was not in question for this event.

Another possible contributing environmental factor, but on a larger scale, would be the magnitude of synoptic forcing and the possible release of potential instability. King et al. (2017) and Sherburn and Parker (2014) discussed how cool season HSLC QLCS events often rely heavily on the synoptic environment and associated deep-layer forcing. The intensity of the synoptic wave, discussed in the previous synoptic analysis section, likely contributed significant amounts of forcing to maintain the QLCS in such a poor thermodynamic environment. A relationship has also been shown to exist between mid-level dry air intrusions and the release of potential instability (Lane and Moore 2006). Several aircraft profiles on the KCLT ACARS soundings started to indicate the arrival of drier mid-level air in the 700-400 mb layer. Any resulting release of potential instability may have contributed to more buoyancy than assessed, however this remains indeterminate.

*(iii) Tornadogenesis via Release of HSI*

Recent work by Goodnight et al. (2022) identifies two primary processes that lead to QLCS tornadogenesis within line-embedded mesovortices; one that is dominated by a release of HSI and one by a pre-tornadic mesocyclone. The authors theorize that the Claremont Tornado occurred primarily via the release of HSI, which plays several key roles regarding anticipation and detectability of the tornado. For QLCSs, mesoscale convergence along the leading edge of the cold pool helps to stretch planetary vorticity into prefrontal strips of vertical vorticity. HSI is a type of barotropic instability that converts the horizontal shear and associated strips of vertical vorticity into discrete, like-signed vortices. The resulting pattern of vorticity is strongest near the surface and drops off quickly with height, which can be seen in radar observations as shallow mesovortices along the leading edge of the QLCS. The transition from shear vorticity to discrete mesovortices occurs quickly on a time scale of 5 to 15 minutes, resulting in rapid tornadogenesis that is extremely difficult for forecasters to anticipate. Pre-tornadic frontogenesis, as is the case for the Claremont

Tornado, has also been shown to be common for cool season HSI tornadogenesis cases, which suggests a more significant role of the larger-scale forcing in QLCS development as well as in the vertical vorticity that fosters the HSI tornadogenesis process.

One of the more challenging aspects of QLCS HSI tornadogenesis is that the theoretical basis for the Three Ingredients Method developed by Schaumann and Przybylinski (2012) originates from modeling studies of QLCS tornadoes that form via the pre-tornadic mesocyclone process with mid-level mesocyclones that are present before tornadogenesis. The pre-tornadic mesocyclone process is inherently more detectable with the Three Ingredients Method performing well when this is the dominant QLCS tornadogenesis mechanism. The utility of the Three Ingredients Method for the anticipation of HSI QLCS tornadoes is less certain. A local surge in the gust front, which is one of the three ingredients, is coincident with the release of HSI which may be the effect of ongoing tornadogenesis due to HSI rather than a cause for it. Additional case studies of QLCS HSI tornadogenesis by Goodnight et al. (2022) further show that HSI QLCS tornadoes can frequently occur without fulfilling all three ingredients. This would explain why the Three Ingredients Method and QLCS Mesovortex Warning System fail to anticipate the Claremont Tornado. The shallow nature of HSI mesovortices and rapid tornadogenesis process results in poor warning statistics with only 30% of HSI tornadoes in the Goodnight et al. (2022) study being warned.

Based on the subtle changes in the environment and HSI tornadogenesis process discussed in the subsections above, the overarching hypothesis for tornadic development is as follows.

A strongly forced QLCS propagated from the Upstate of South Carolina northeast into the foothills of western North Carolina. Initially, the QLCS was elevated above a cold and stable CAD wedge, but it approached the warm front and open warm sector which was in place over the eastern third of Catawba County. The SPC mesoanalysis and the WoFS both underestimated the temperature and dewpoint in the warm sector by several degrees. Increased moisture along the warm front aided by the frontogenetical circulation contributed to a narrow axis of enhanced moisture/theta-e along the warm front with the nose of the theta-e ridge extending into northeast Catawba County. The increase in moisture had implications on the available instability, which while limited, was non-zero.

While only 70 J $kg^{-1}$ of SBCAPE, which was focused in a shallow and weakly unstable layer, was sampled on the KCLT ACARS, local storm-scale processes were likely able to overcome the temperature inversion and tap into elevated MUCAPE aloft. Exactly how much instability was realized across Catawba County remains uncertain, but apparently there was sufficient instability to support vortex stretching and tornadogenesis. As the QLCS crossed the warm front and became surface-based on the warm side of the boundary it encountered this favorable environment. The portion of the line moving through Catawba County was favorably oriented with the surface-to-3 km shear vectors with a balance between the cold pool and environmental shear. Tornadogenesis via release of HSI happened rapidly as the QLCS crossed the narrow tongue of moisture pooling.

## 5. Summary, Recommendations, and Future Work

A powerful storm system impacted northeast Georgia and the Carolinas on 9 January 2024. A line of thunderstorms, some of which were severe, moved across the Upstate of South Carolina and into the foothills of western North Carolina during the morning to early afternoon hours. A deadly EF-1 tornado occurred in the Claremont, North Carolina, community north of the tornado watch that was in effect and in the absence of a tornado warning. The tornado occurred in a highly anomalous environment characterized by extreme values of low- and deep-layer vertical wind shear and what was assessed to be negligible instability in a very poor thermodynamic environment. Traditional mesoanalysis and radar interrogation techniques combined with an established conceptual model for QLCS tornadoes determined that the environment was not supportive of tornadic development. Storm motions were also very fast with the tornadogenesis process occurring rapidly over five minutes or less. This created an extremely challenging warning environment for even the most experienced forecasters with the Three Ingredients Method and QLCS Mesovortex Warning System, commonly utilized during QLCS events, unable to anticipate tornadogenesis.

Post-event review determined that SPC mesoanalysis fields and the WoFS underestimated a narrow, weakly unstable axis of increased moisture against a warm front separating a CAD wedge from an open warm sector. This was supported by the KCLT ACARS sounding which sampled a very shallow weakly unstable layer with non-zero values of

SBCAPE along with elevated MUCAPE rooted above a temperature inversion. The authors hypothesize that a portion of the strongly forced QLCS, favorably aligned with surface-to-3 km shear vectors, crossed the warm front with local storm-scale processes eroding the temperature inversion and tapping into MUCAPE aloft, thus taking advantage of a narrow ridge of enhanced moisture/instability with a tornado rapidly occurring via release of HSI. Extremely shallow QLCS tornadoes in such marginal thermodynamic environments present one of the most challenging warning scenarios a forecaster may ever be faced with. Historically, based on the dataset compiled by Goodnight et al. (2022), HSI QLCS tornadoes are only warned 30% of the time, thus presenting an area needing additional research and improvement.

Several recommendations are identified that can be implemented into severe weather operations. It is highly recommended that forecasters compare actual observations to the SPC mesoanalysis and model analysis fields and identify any errors in model initializations and forecasts. This is especially key in HSLC environments where even 40-50 J $kg^{-1}$ of SBCAPE can make a difference between tornadic and non-tornadic convection. Identifying exact locations of boundaries is also imperative, with a focus on front crossing convection. An update to the QLCS tornado conceptual model is also recommended, with the caveats of the Three Ingredients Method and QLCS Mesovortex Warning System during cases of shallow HSI tornadoes being documented. From a radar/warning perspective, it is also recommended to err on the side of caution in strongly forced anomalous HSLC environments when instability is in question. Tornado warnings should not be issued well into the stable CAD wedge, but if the storm is no longer elevated above the CAD inversion and is near/crossing a warm front, a tornado warning should be issued if the mechanisms are present for tornadogenesis despite uncertainty regarding thermodynamic profiles.

Given limited near-storm observational data, the hypothesis for tornadic development presented by the authors cannot be confirmed at this time. As such, future work will focus on collaborating with a university to pursue high-resolution modeling of the QLCS in order to verify what mechanisms allowed for tornadogenesis and the validity of the hypothesis.

## 6. References

Bailey, C.M., G. Hartfield, G.M. Lackmann, K. Keeter, and S. Sharp, 2003: An Objective Climatology, Classification Scheme, and Assessment of Sensible Weather Impacts for Appalachian Cold-Air Damming. *Wea. Forecasting*, **18**, 641-661, https://doi.org/10.1175/1520-0434(2003)018<0641:AOCCSA>2.0.CO;2.

Benjamin, S.G., B.E. Schwartz, and R.E. Cole, 1999: Accuracy of ACARS Wind and Temperature Observations Determined by Collection. *Wea. Forecasting*, **14**, 1032-1038, https://doi.org/10.1175/1520-0434(1999)014<1032:AOAWAT>2.0.CO;2.

Coleman, T.A., A.W. Lyza, K.R. Knupp, K. Laws, and W. Wyatt, 2018: A Significant Tornado in a Heterogeneous Environment During VORTEX-SE. *J. Severe Storms Meteor.*, **13**, 1-25, https://doi.org/10.55599/ejssm.v132i2.70.

Davies, J.M., 2004: Estimations of CIN and LFC Associated with Tornadic and Nontornadic Supercells. *Wea. Forecasting*, **19**, 714-726, https://doi.org/10.1175/1520-0434(2004)019<0714:EOCALA>2.0.CO;2.

Davis, J.M., and M.D. Parker, 2014: Radar Climatology of Tornadic and Nontornadic Vortices in High-Shear, Low-CAPE Environments in the Mid-Atlantic and Southeastern United States. *Wea. Forecasting*, **29**, 828-853, https://doi.org/10.1175/WAF-D-13-00127.1.

Goodnight, J.S., D.A. Chehak, and R.J. Trapp, 2022: Quantification of QLCS Tornadogenesis, Associated Characteristics, and Environments across a Large Sample. *Wea. Forecasting*, **37**, 2087-2105, https://doi.org/10.1175/WAF-D-22-0016.1.

Guyer, J.L., and A.R. Dean, 2010: Tornadoes Within Weak CAPE Environments Across the Continental United States. *25th Conf. on Severe Local Storms*, Denver, CO, Amer. Meteor. Soc., 1.5, https://ams.confex.com/ams/25SLS/webprogram/Paper175725.html.

Hampshire, N.L., R.M. Mosier, T.M. Ryan, and D.E. Cavanaugh, 2018: Relationship of Low-Level Instability and Tornado Damage Rating Based on Observed Soundings. *J. Operational Meteor.*, **6**, 1-12, https://doi.org/10.15191/nwajom.2018.0601.

Heinselman, P. L., and Coauthors, 2023: Warn-on-Forecast System: From Vision to Reality. *Wea. Forecasting*, **39**, 75–95, https://doi.org/10.1175/WAF-D-23-0147.1.

King, J.R., M.D. Parker, K.D. Sherburn, and G.M. Lackmann, 2017: Rapid Evolution of Cool Season, Low-CAPE Severe Thunderstorm Environments. *Wea. Forecasting*, **32**, 763-779, https://doi.org/10.1175/WAF-D-16-0141.1.

Kosiba, K. A., and Coauthors, 2024: The Propagation, Evolution, and Rotation in Linear Storms (PERiLS) Project. *Bull.Amer.Meteor.Soc.*, **22**, E1768-E1799, https://doi.org/10.1175/BAMS-D-22-0064.1.

Lackmann, G.M., and W.M. Stanton, 2004: Cold-Air Damming Erosion: Physical Mechanisms, Synoptic Settings, and Model Representation. *20th Conf. on Weather Analysis and Forecasting*, Seattle, WA, Amer. Meteor. Soc., 18.6, https://ams.confex.com/ams/84Annual/techprogram/paper_73411.htm

Lane, J.D., and P.D. Moore, 2006: Observations of a Non-Supercell Tornadic Thunderstorm From Terminal Doppler Weather Radar. *23rd Conf. on Severe Local Storms,* St. Louis, MO, Amer. Meteor. Soc. P4.5, https://ams.confex.com/ams/pdfpapers/115102.pdf.

Lovell, L.T., and M.D. Parker, 2022: Simulated QLCS Vortices in a High-Shear, Low-CAPE Environment. *Wea. Forecasting*, **37**, 989-1012, https://doi.org/10.1175/WAF-D-21-0133.1.

McAvoy, B.P., W.A. Jones, and P.D. Moore, 2000: Investigation of an Unusual Storm Structure Associated With Weak to Occasionally Strong Tornadoes Over the Eastern United States. Preprints, *20th Conf. on Severe Local Storms,* Orlando, FL, Amer. Meteor. Soc., 182-185, http://www.erh.noaa.gov/gsp/localdat/ConfPapers/Broken-S.pdf.

McCaul, E.W., and M.L. Weisman, 2001: The Sensitivity of Simulated Supercell Structure and Intensity to Variations in the Shapes of Environmental Buoyancy and Shear Profiles. *Mon. Wea. Rev.*, **129**, 664-687, https://doi.org/10.1175/1520-0493(2001)129<0664:TSOSSS>2.0.CO;2.

Park, S.G., V.N. Bringi, V. Chandrasekar, M. Maki and K. Iwanami, 2005: Correction of Radar Reflectivity and Differential Reflectivity for Rain Attenuation at X Band. Part I: Theoretical and Empirical Basis. *J. Atmos. Oceanic Technol.*, **22**, 1621-1632, https://doi.org/10.1175/JTECH1803.1.

Przybylinski, R.W., G.K. Schmocker, and Y.J. Lin, 2000: A Study of Storm and Vortex Morphology During the 'Intensifying Stage' of Severe Wind Mesoscale Convective Systems. Preprints, *20th Conf. on Severe Local Storms,* Orlando, FL. Amer. Meteoro. Soc., 173-176.

Schaumann, J.S., and R.W. Przybylinski, 2012: Operational Application of 0-3 km Bulk Shear Vectors in Assessing Quasi Linear Convective System Mesovortex and Tornado Potential. *26th Conf. on Severe Local Storms*, Nashville, TN, Amer. Meteor. Soc., 142, https://ams.confex.com/ams/26SLS/webprogram/Paper212008.html.

Sherburn, K.D., and M.D. Parker, 2014: Climatology and Ingredients of Significant Severe Convection in High-Shear, Low CAPE Environments. *Wea. Forecasting*, **29**, 854-877, https://doi.org/10.1175/WAF-D-13-00041.1.

——, ——, J.R. King, and G.M. Lackmann, 2016: Composite Environments of Severe and Nonsevere High-Shear, Low-CAPE Convective Events. *Wea. Forecasting*, **31**, 1899-1927, https://doi.org/10.1175/WAF-D-16-0086.1.

Trapp, R.J., E.D. Mitchell, G.A. Tipton, D.W. Effertz, A.I. Watson, D.L. Andra Jr., and M.A. Magsig, 1999: Descending and Nondescending Tornadic Vortex Signatures Detected by WSR-88Ds. *Wea. Forecasting*, **14**, 625-639, https://doi.org/10.1175/1520-0434(1999)014<0625:DANTVS>2.0.CO;2.

## 7. Figures and Tables

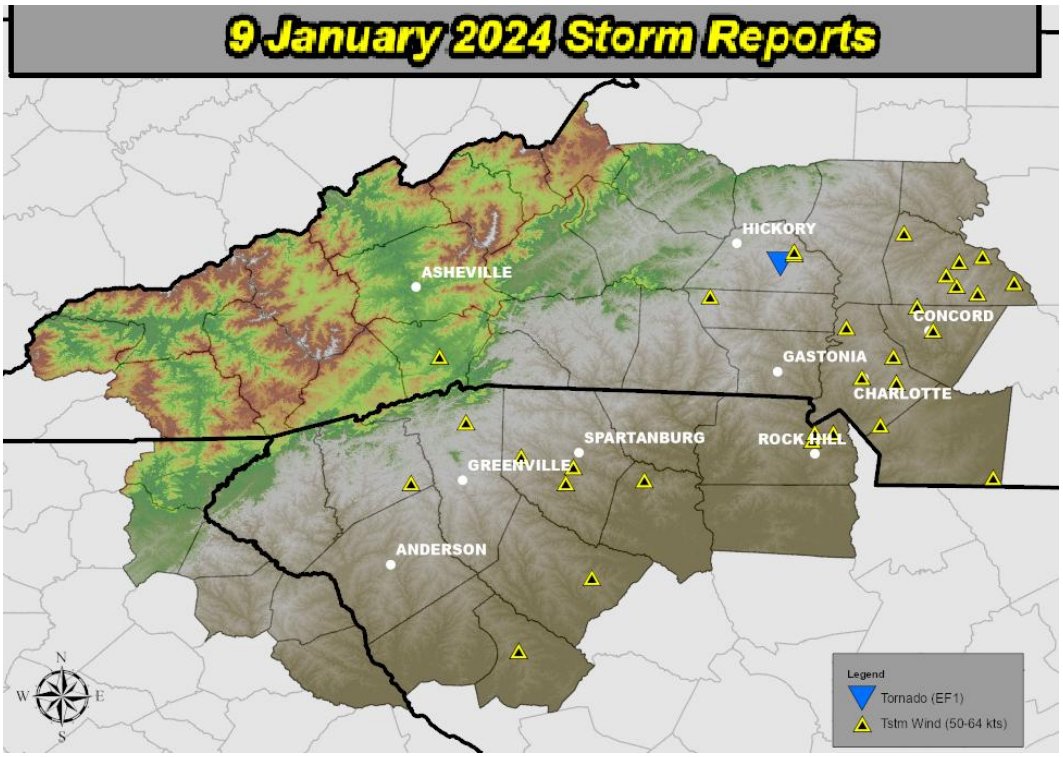


**Fig. 1.** Local storm reports received for the 24-hour period from 1200 UTC on 9 January to 1200 UTC on 10 January 2024 (NWS Storm Prediction Center). The white upside-down triangle denotes the start of the Claremont Tornado track. Black and yellow triangles show locations of wind damage reports.

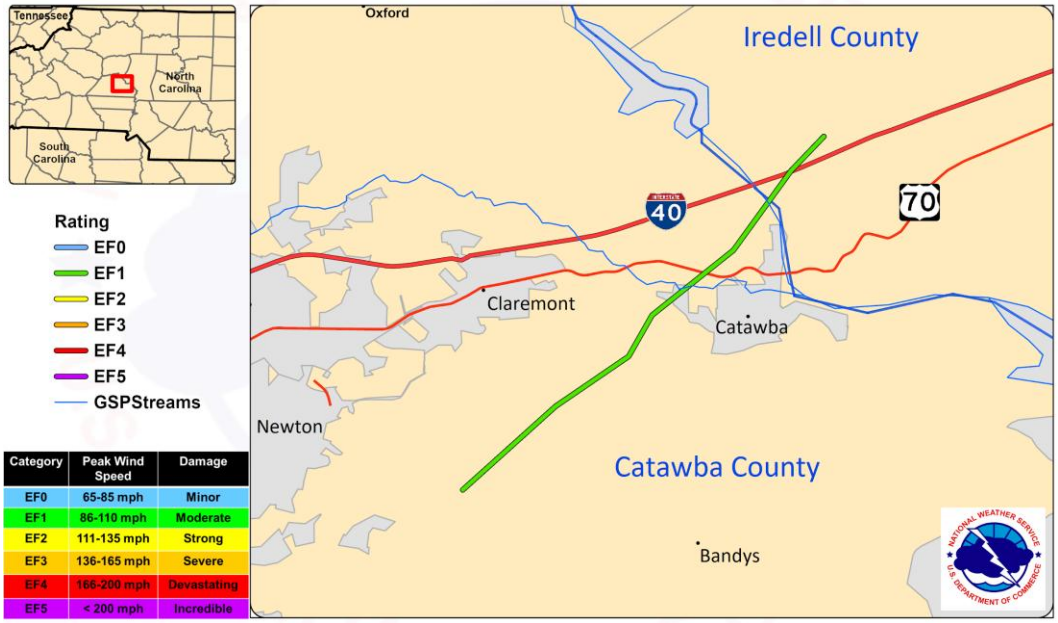


**Fig. 2.** Path of the Claremont Tornado (thick green line) across eastern Catawba and western Iredell counties on 9 January 2024.

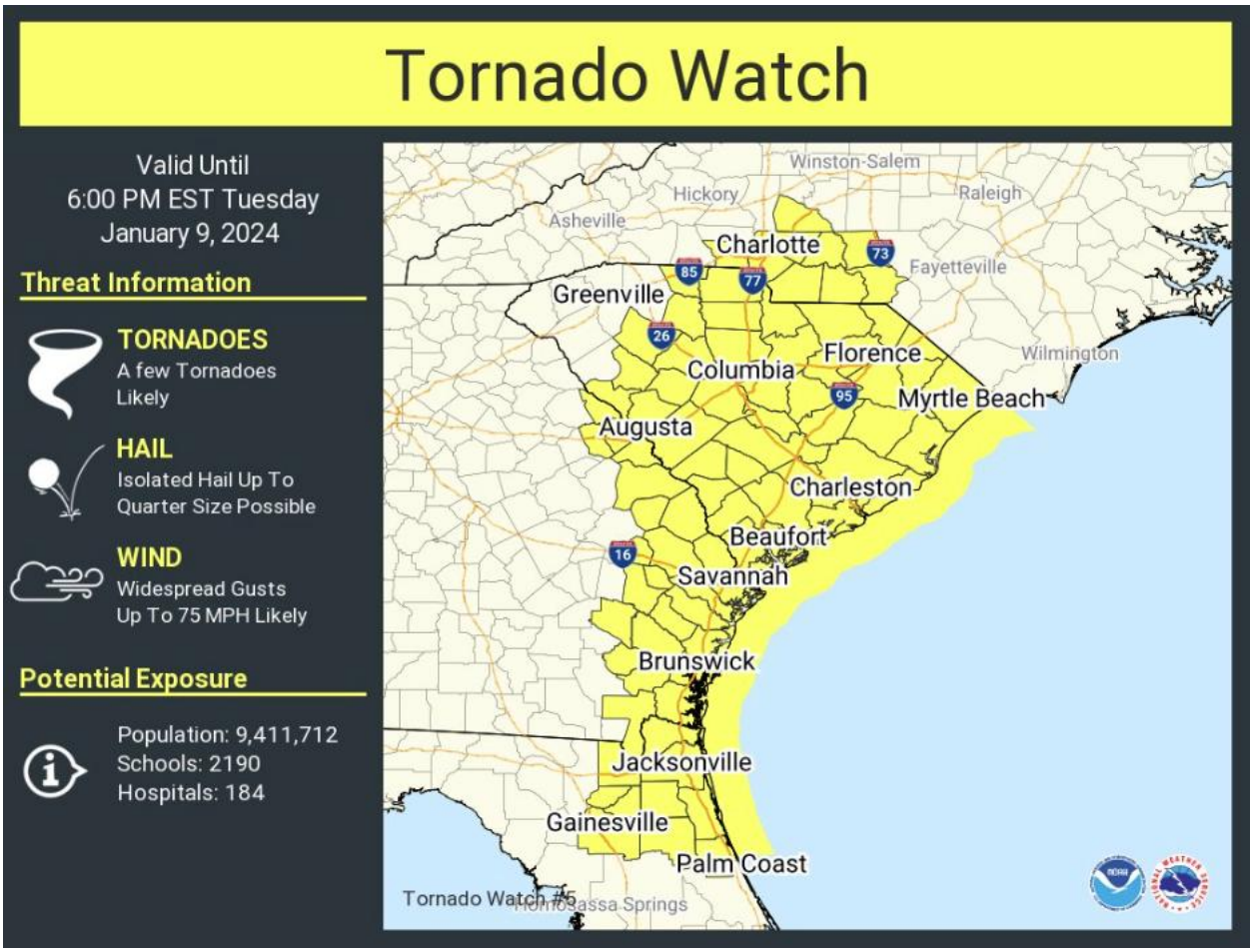


**Fig. 3.** Tornado Watch (#5) issued by the Storm Prediction Center at 1640 UTC valid until 2300 UTC on 9 January 2024. Counties included in the Tornado Watch are highlighted in yellow.

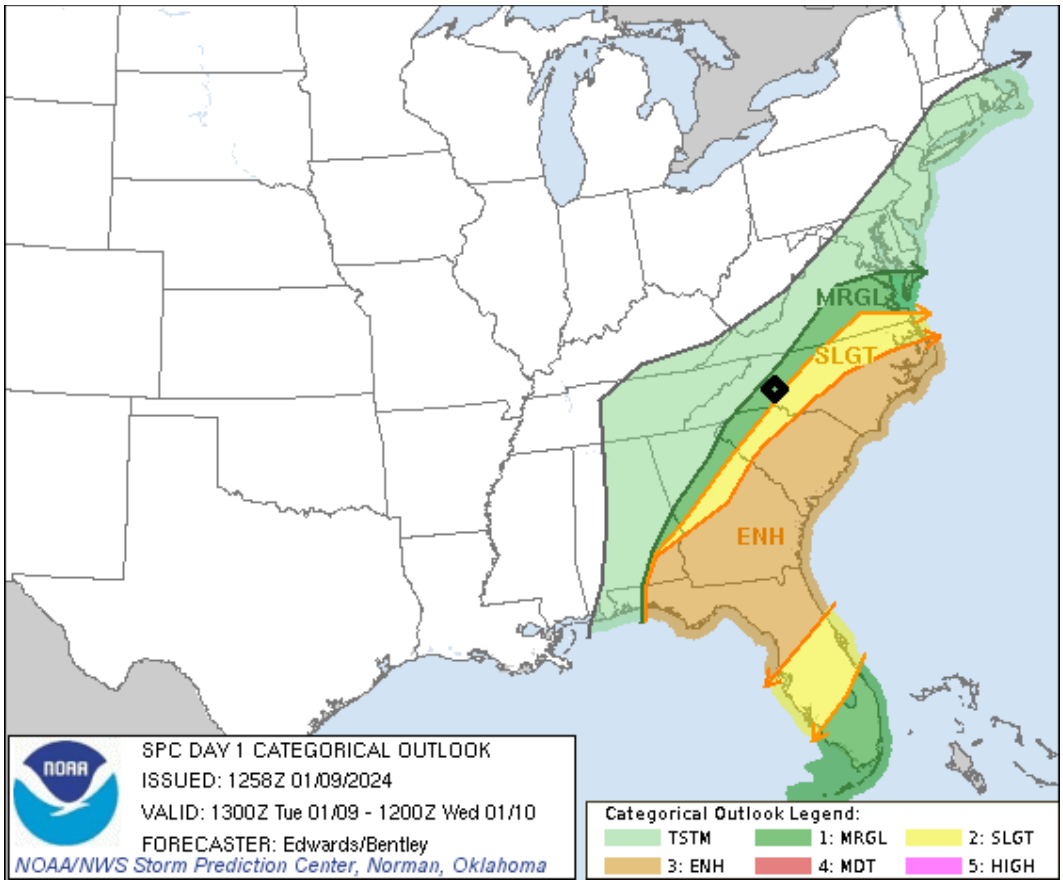


**Fig. 4.** Day 1 Convective Outlook issued by the Storm Prediction Center at 1258 UTC on 9 January 2024 for the period 1300 UTC on 9 January to 1200 UTC on 10 January. The black diamond indicates the approximate location of the Claremont Tornado. Risk categories given according to the legend at the lower right of the figure.

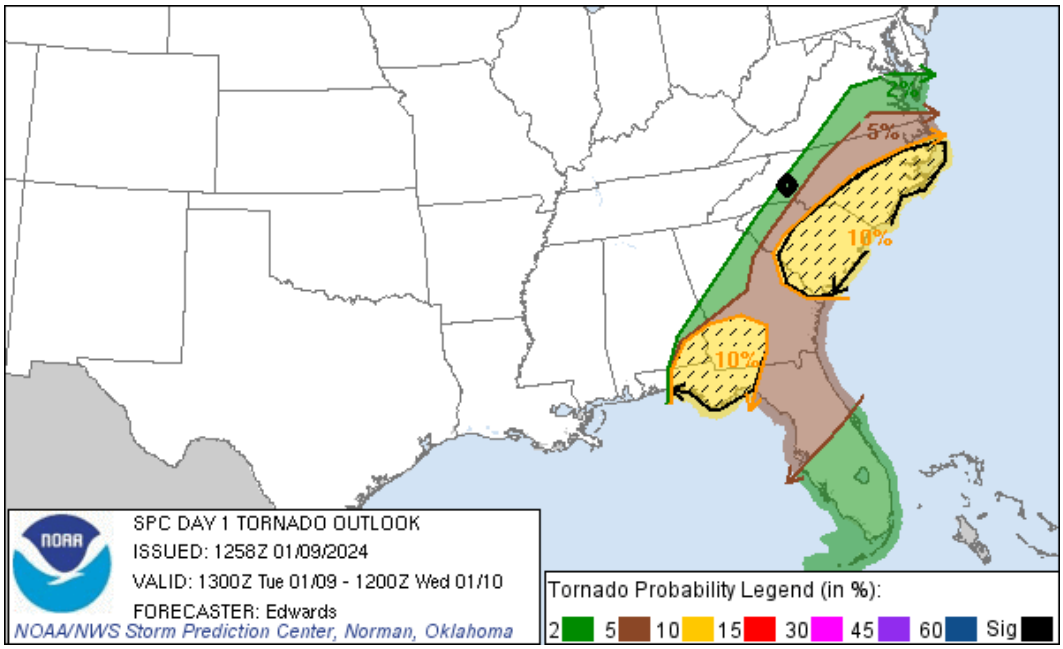


**Fig. 5.** Tornado probabilities on the Day 1 Convective Outlook issued by the Storm Prediction Center at 1258 UTC on 9 January 2024, for the period 1300 UTC on 9 January to 1200 UTC on 10 January. Hatched areas denote the possibility of a significant tornado (damage EF-2 or greater). The black diamond indicates the approximate location of the Claremont Tornado.

**Fig. 6.** SPC objective analysis of 250 mb observations, streamlines (black lines with arrows showing direction), and isotachs (kt; gray contours and color fill) at (A) 1200 UTC 8 January 2024, and (B) 1200 UTC 9 January 2024, and 500 mb observations, geopotential height (dam; gray contours),

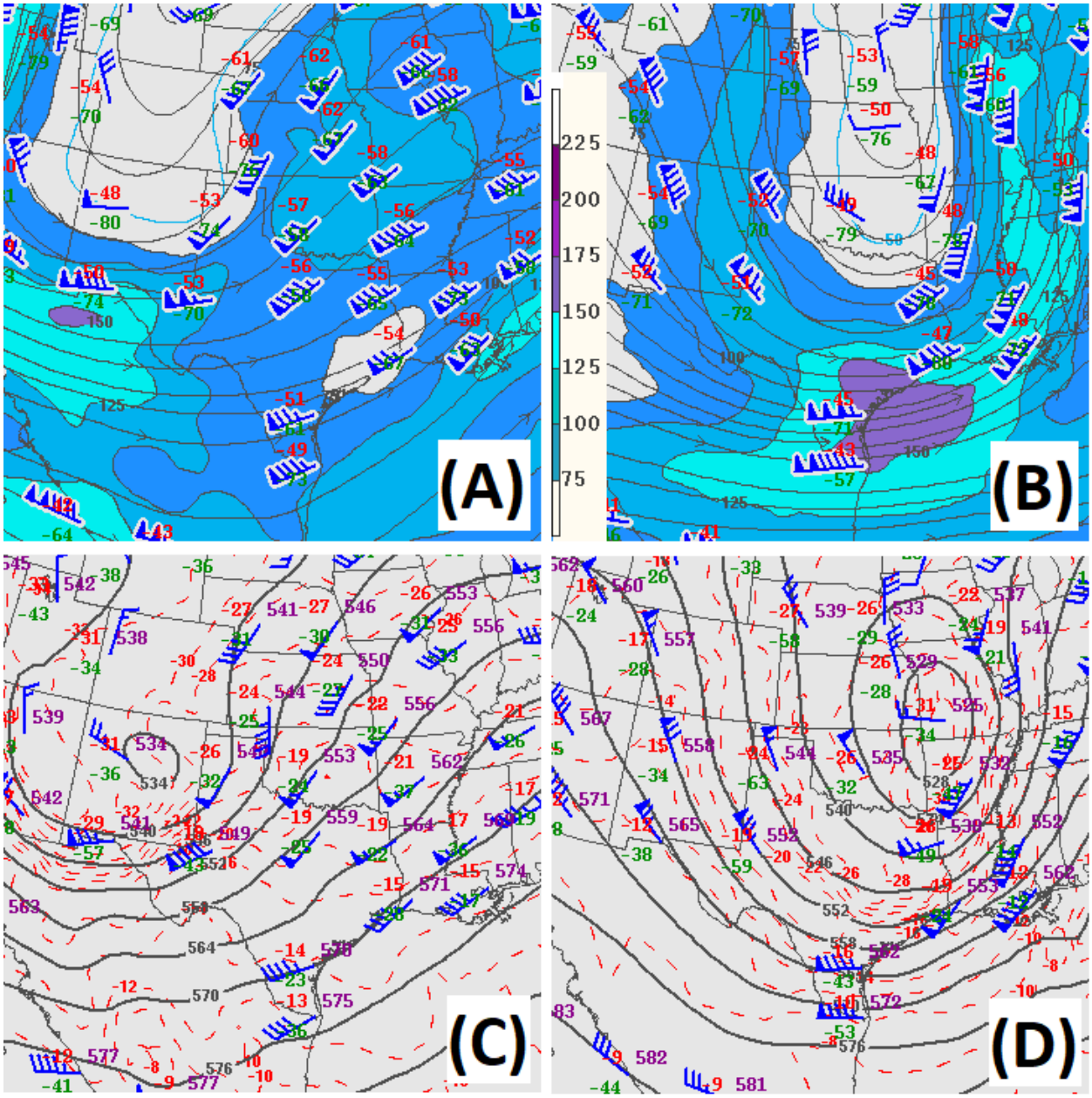


isotherms (ºC; dashed red contours), and wind (kt; barbs) at (C) 1200 UTC 8 January 2024, and (D) 1200 UTC 9 January 2024.

**Fig. 7.** SPC objective analysis of (A) 300 mb observations, streamlines (black lines with arrows showing direction), isotachs (kt; gray contours and color fill), wind (kt; barbs), and divergence ($s^{-1}$;yellow contours), (B) 500 mb observations, geopotential height (dam; gray contours), isotherms (ºC; dashed red contours), and wind (kt; barbs), (C) 700 mb observations, geopotential height (dam; gray contours), temperature (ºC isotherms; blue and red dashed contours), dew point (ºC; green contours greater than and

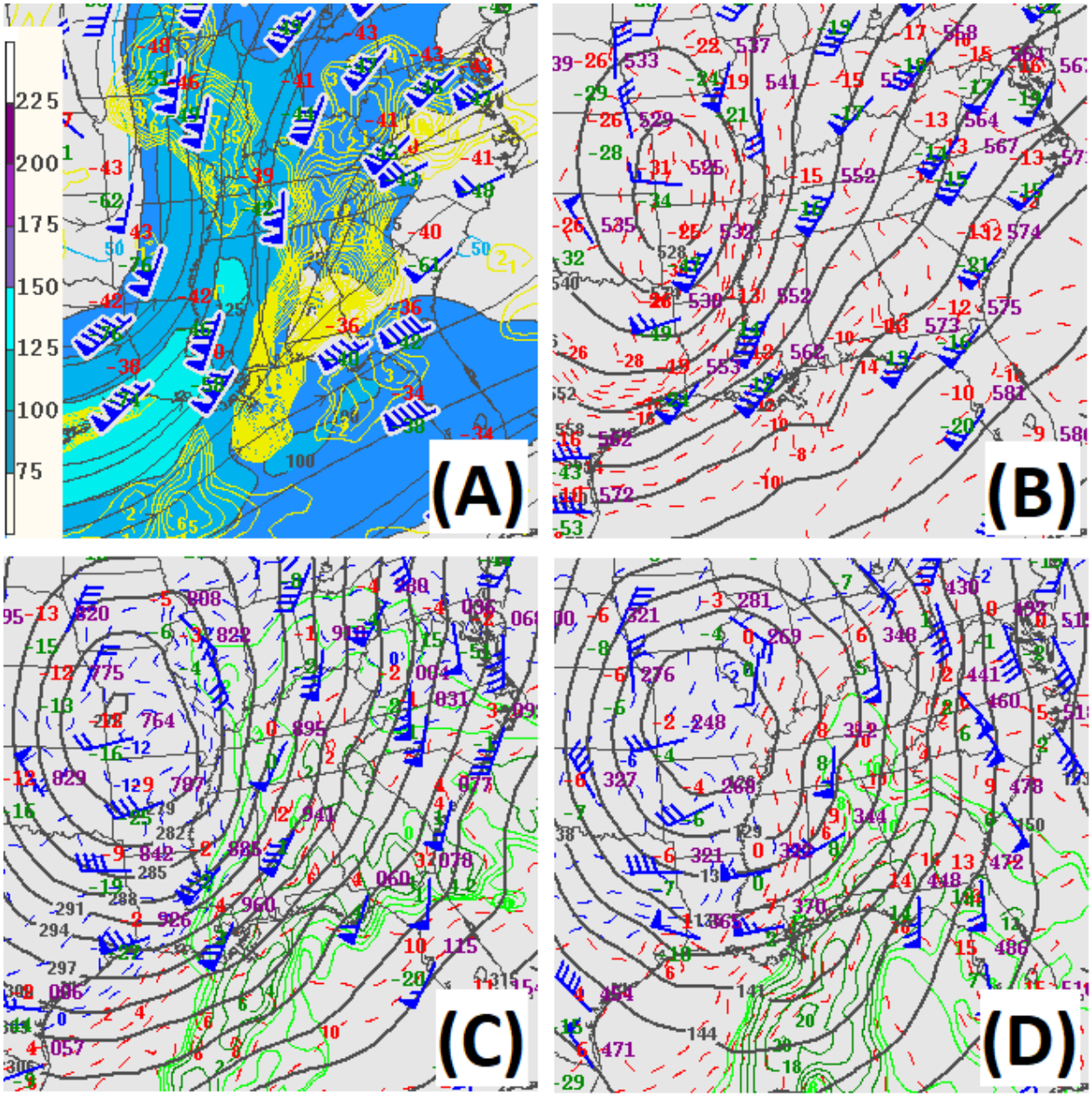


equal to -4 ºC), and wind (kt; barbs), and (D) 850 mb observations, geopotential height (dam; gray contours), temperature (ºC isotherms; blue and red dashed contours), dew point (ºC; green contours greater than and equal to 8 ºC), and wind (kt; barbs) at 1200 UTC on 9 January 2024.

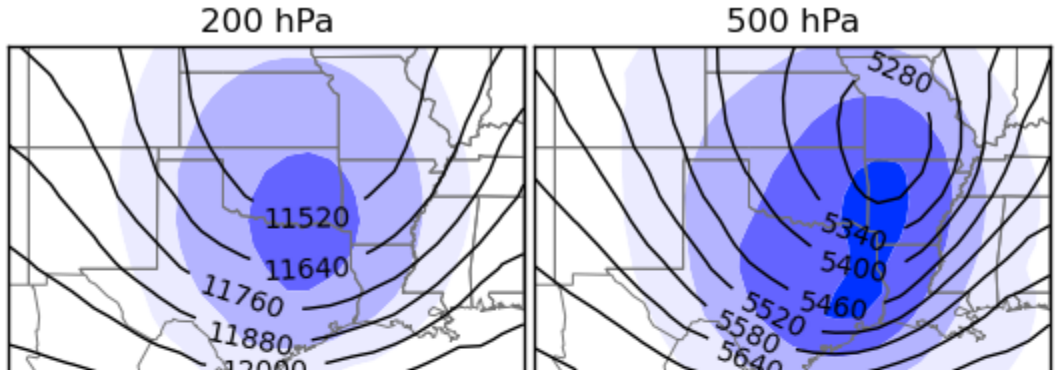

**Fig. 8.** NAEFS initial hour analysis of mean geopotential height (m; black contours) and standardized anomaly (standard deviation; color fill with color bar indicated at the bottom), at 200 mb (upper left), 500 mb (upper right), 700 mb (lower left), and 850 mb (lower right), valid at 1200 UTC on 9 January 2024.

**Fig. 9.** Skew-T, log-P, diagram of upper air observation taken at Greensboro, North Carolina, at 1200 UTC on 9 January 2024. The

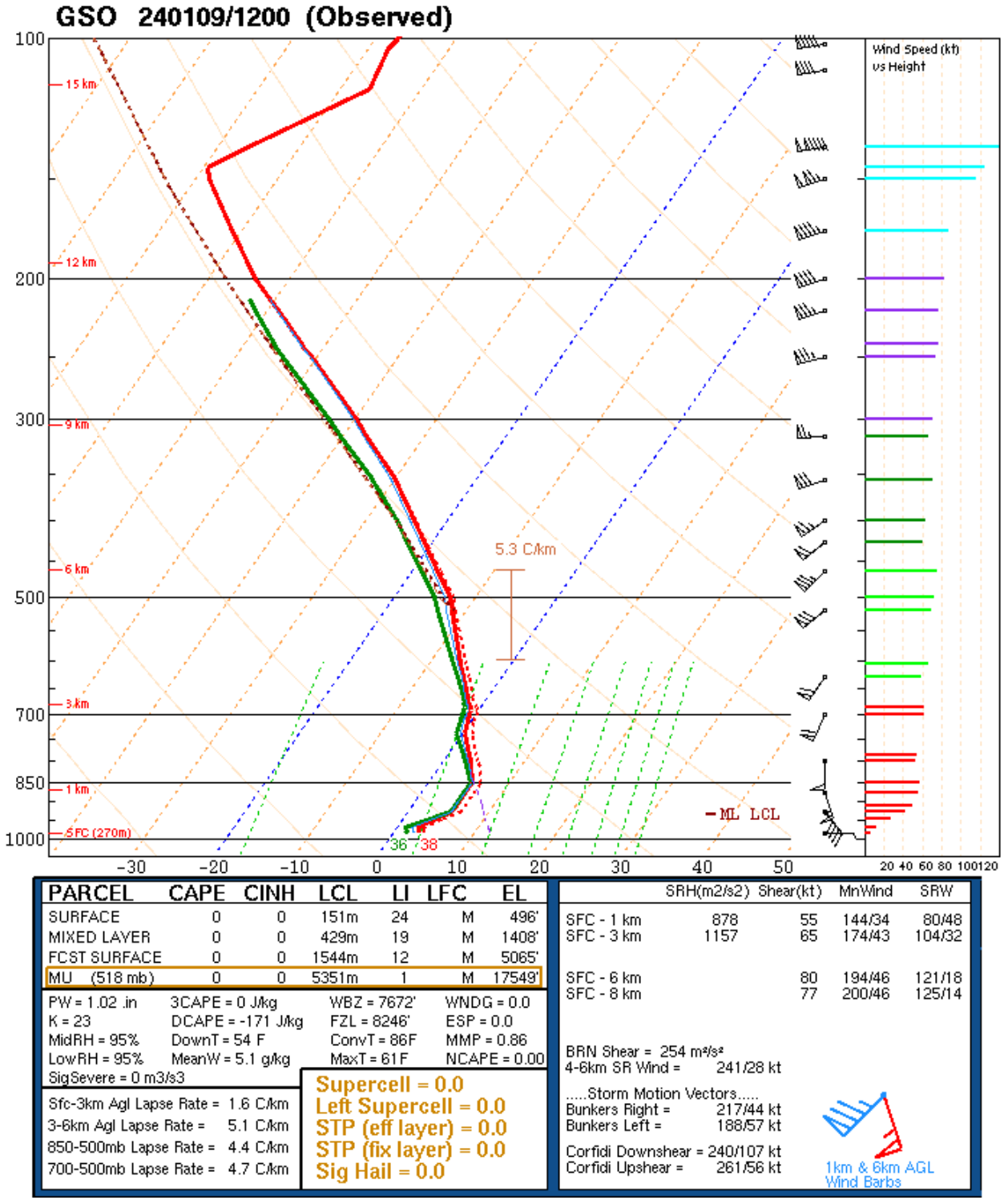


temperature sounding is shown by the thick red line and the dew point sounding by the thick green line.

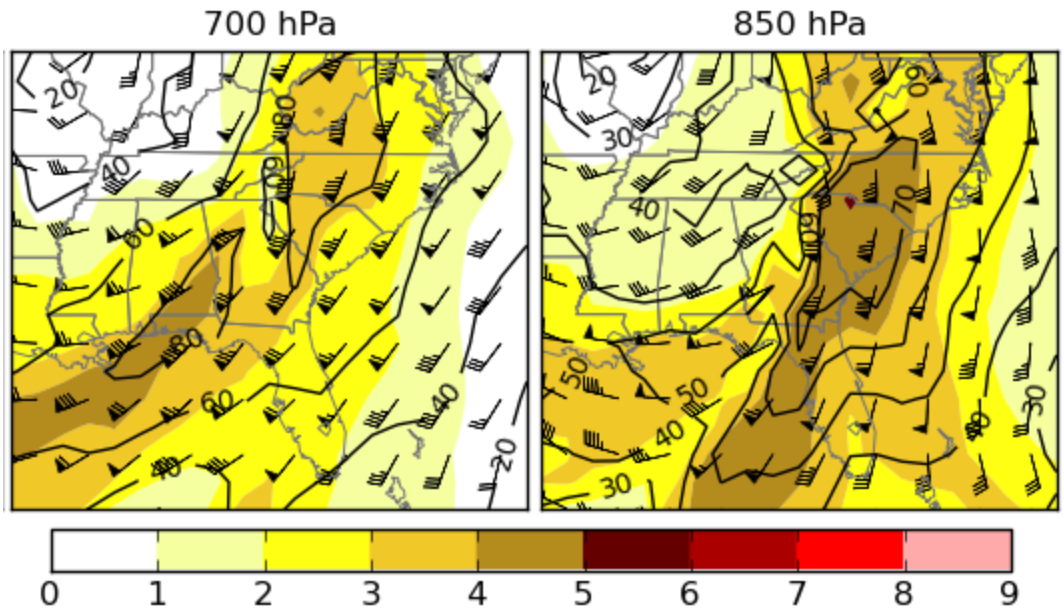


**Fig. 10.** NAEFS 6-hour forecast of mean wind speed (kt; black contours and barbs) and standardized anomaly (standard deviation; color fill with color bar shown at the bottom of the figure) at 700 mb (left) and 850 mb (right), valid 1800 UTC on 9 January 2024.

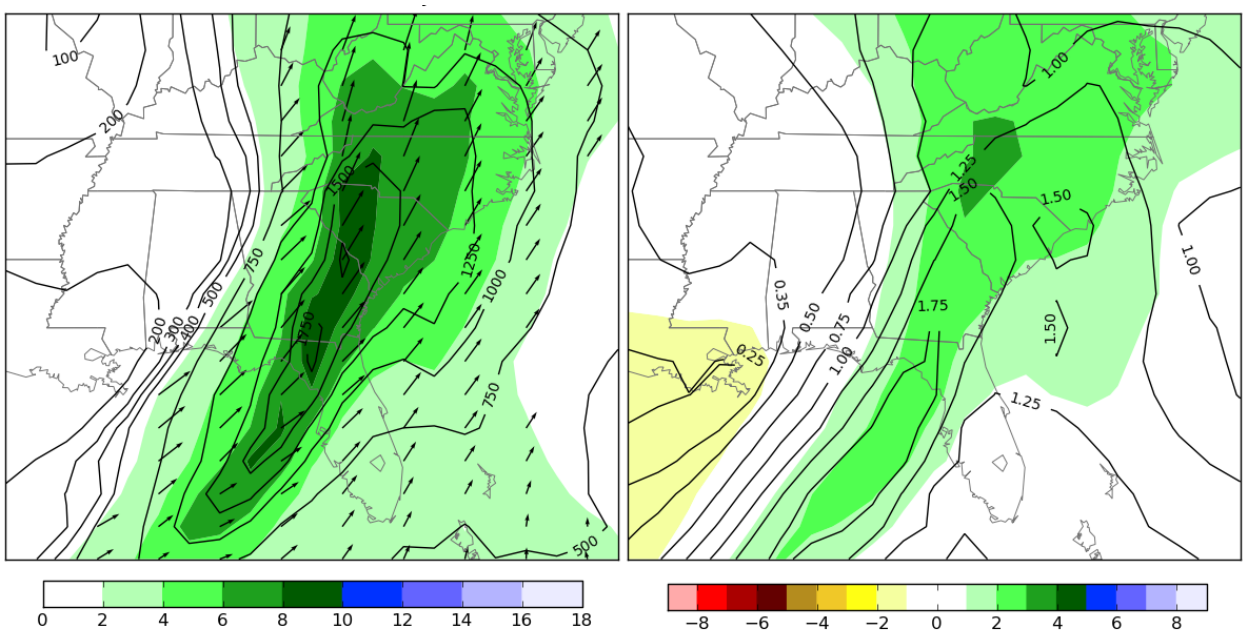


**Fig. 11.** NAEFS 6-hour forecast of (right) mean integrated water vapor transport (kg $m^{-1}s^{-1}$; black contours and arrows) and standardized anomaly (standard deviation; color fill), and (left) precipitable water (in; black contours) and standardized anomaly (standard deviation; color fill), valid 1800 UTC on 9 January 2024.

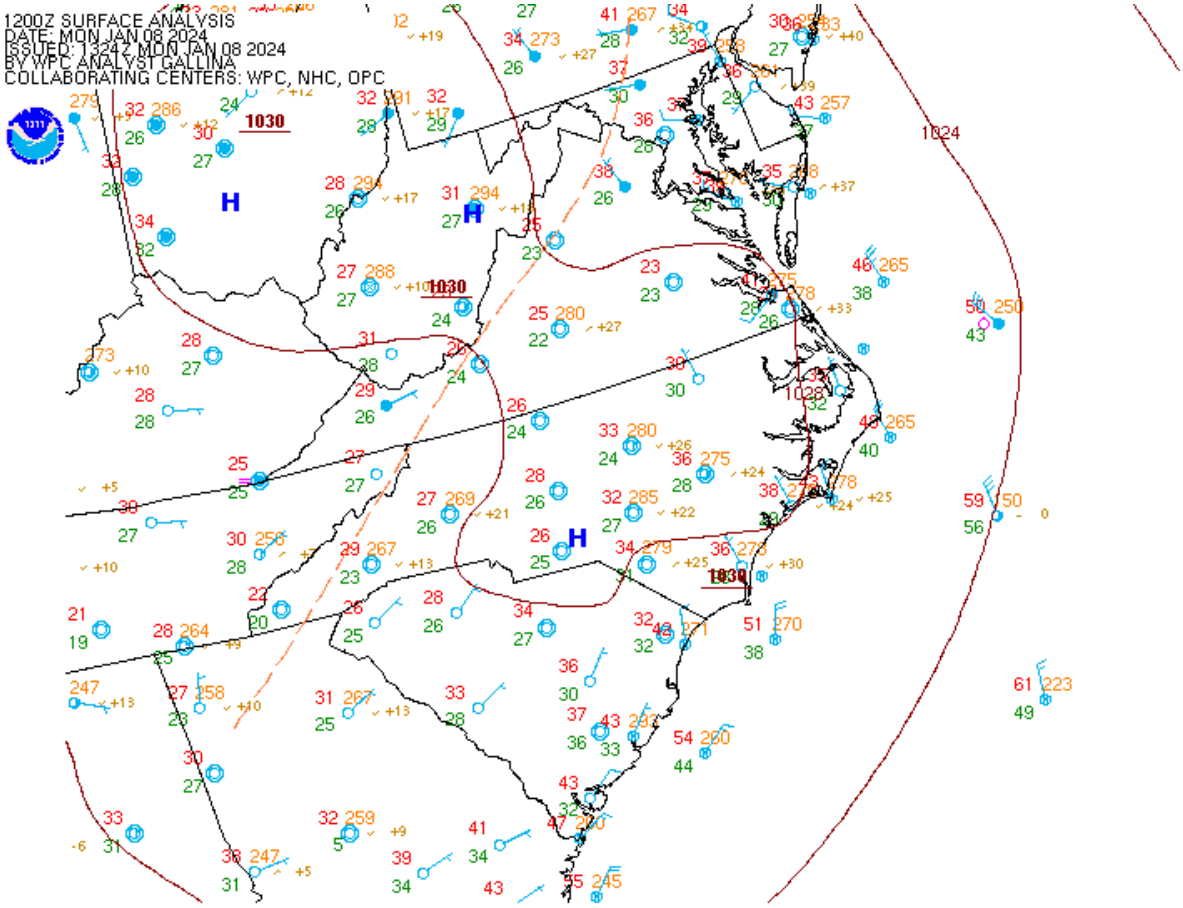


**Fig. 12.** Weather Prediction Center surface analysis of sea level pressure (mb, brown contours), pressure centers, and fronts at 1200 UTC on 8 January 2024. Select surface observations are indicated according to the traditional station model.

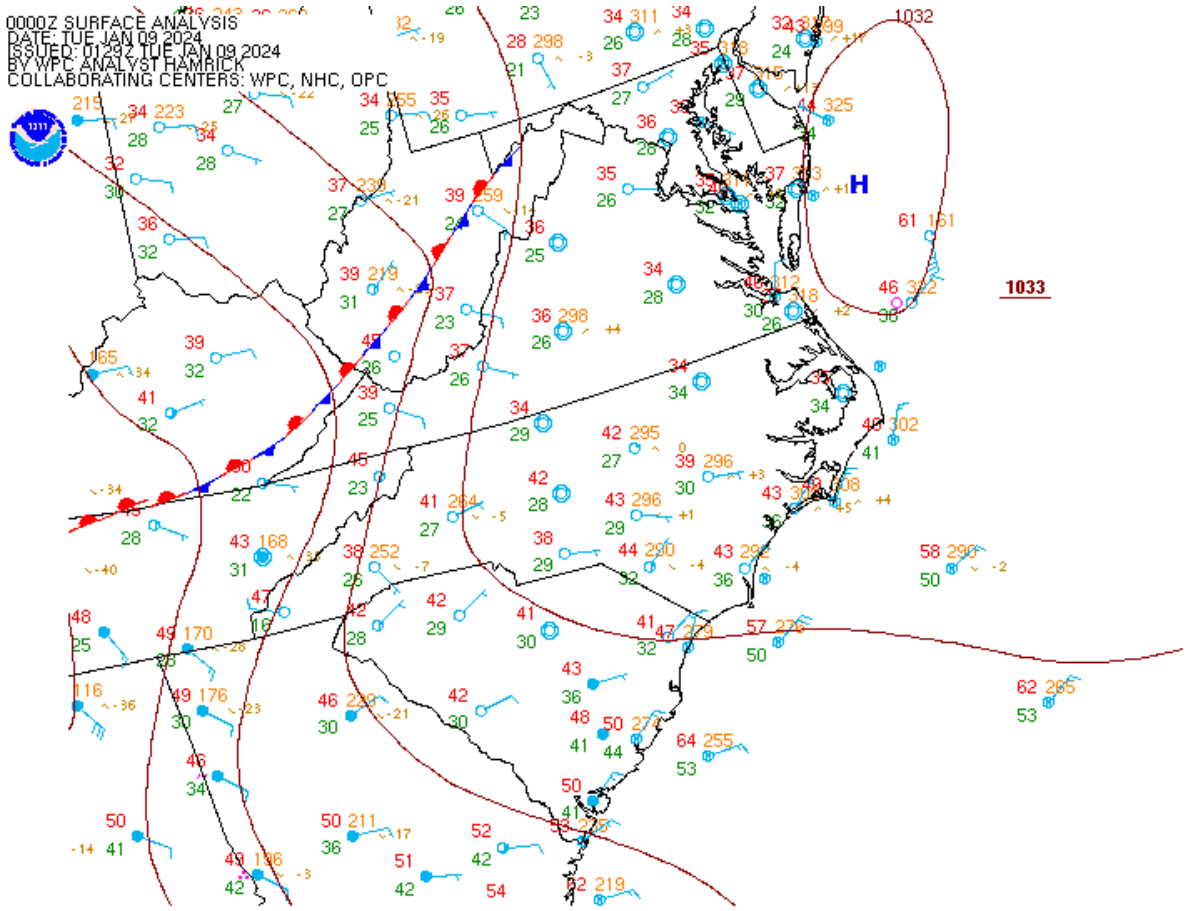


**Fig. 13.** As in Fig. 12, except for 0000 UTC on 9 January 2024.

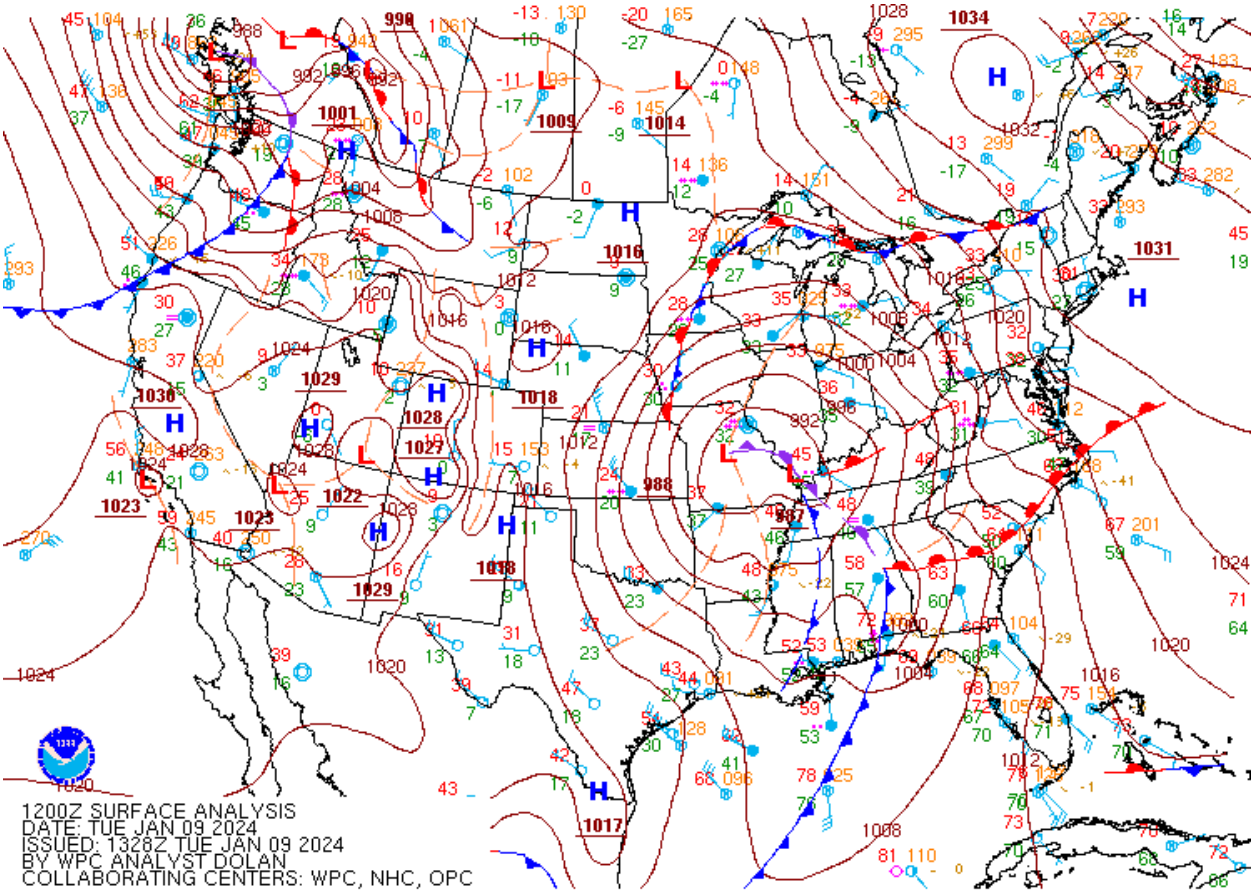


**Fig. 14.** As in Fig. 12, except for 1200 UTC on 9 January 2024.

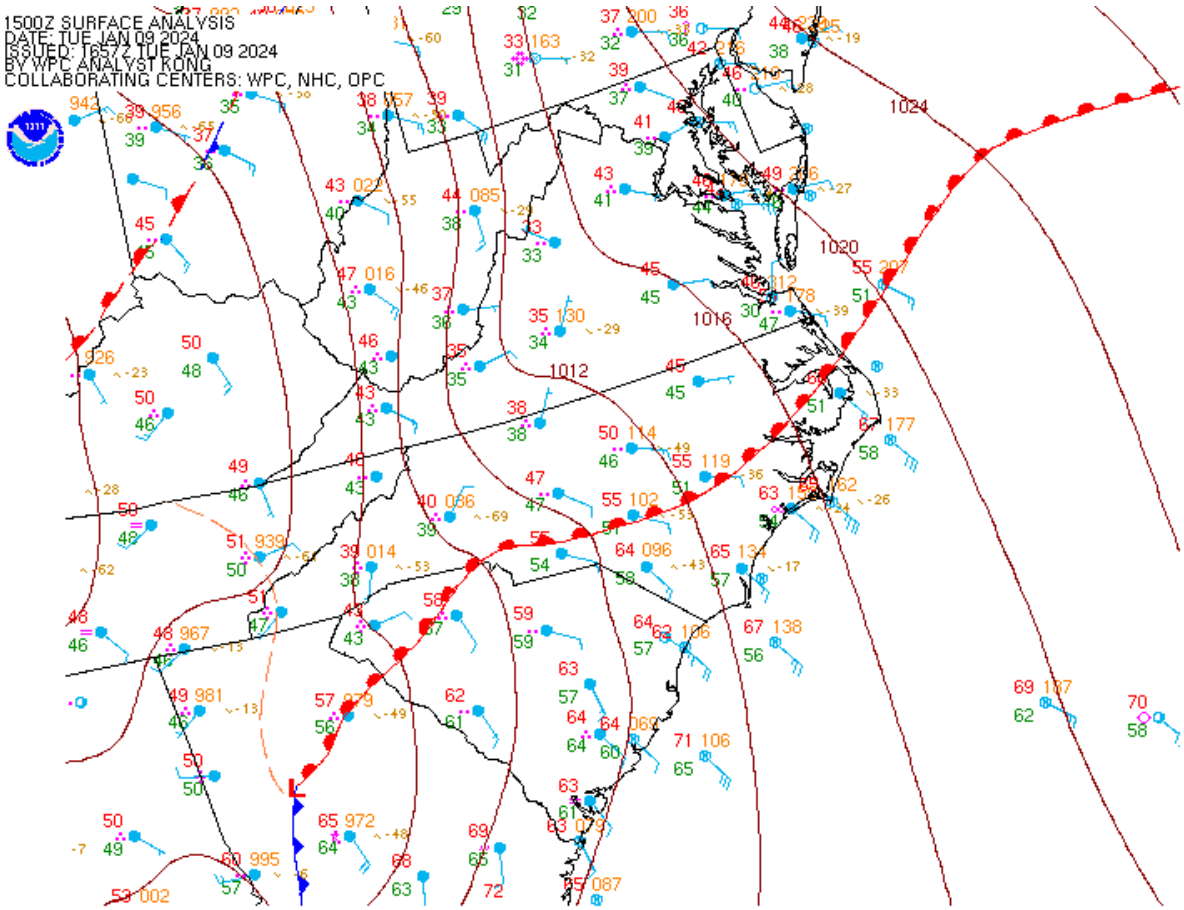


**Fig. 15.** As in Fig. 12, except for 1500 UTC on 9 January 2024.

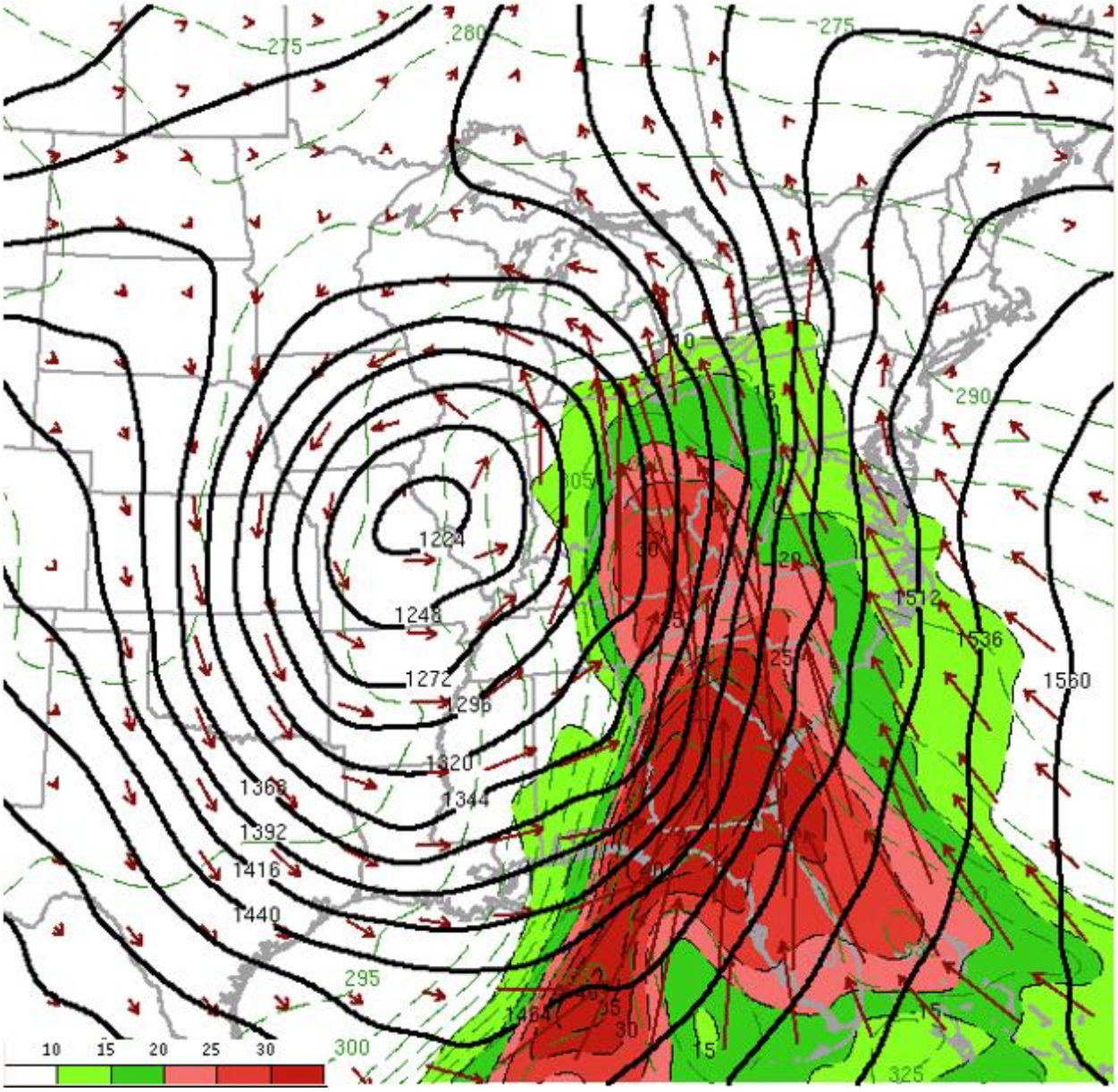


**Fig. 16.** 850 mb moisture transport (m $s^{-1}$; fill and vector), geopotential height (dam; black contours) and equivalent potential temperature (K; dashed green contours) at 1400 UTC 9 January.

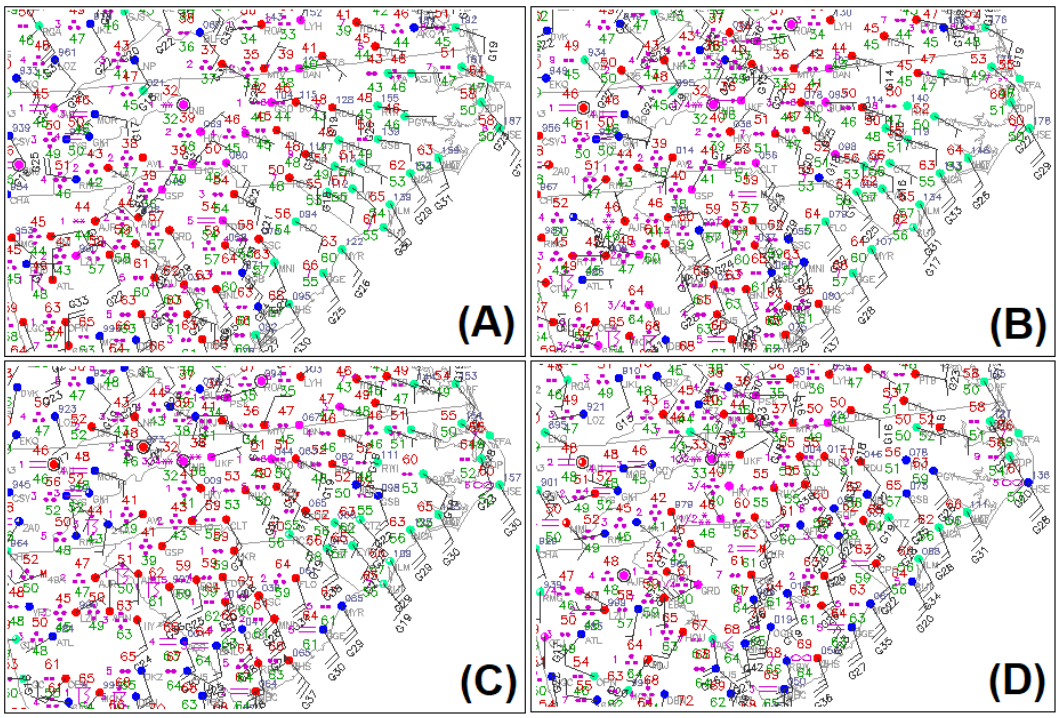


**Fig. 17.** Surface observations at (a) 1400 UTC, (b) 1500 UTC, (c) 1600 UTC, and (d) 1700 UTC on 9 January 2024.

**Table 1.** Five minute observations from Claremont, NC.

| Time | Temperature | Dew Point | Humidity | Wind | Speed | Gust | Pressure | Precip. Rate. | Precip. Accum. |
|---|---|---|---|---|---|---|---|---|---|
| 11:04 AM | 43.3 °F | 42.0 °F | 99 % | East | 2.6 mph | 7.0 mph | 29.34 in | 0.35 in | 1.66 in |
| 11:09 AM | 43.5 °F | 42.0 °F | 99 % | East | 1.3 mph | 7.0 mph | 29.34 in | 0.36 in | 1.68 in |
| 11:14 AM | 43.5 °F | 42.0 °F | 99 % | East | 2.6 mph | 7.0 mph | 29.34 in | 0.37 in | 1.73 in |
| 11:19 AM | 43.3 °F | 42.0 °F | 99 % | East | 1.8 mph | 7.0 mph | 29.32 in | 0.40 in | 1.79 in |
| 11:24 AM | 43.3 °F | 42.0 °F | 99 % | East | 3.8 mph | 7.0 mph | 29.32 in | 0.44 in | 1.85 in |
| 11:29 AM | 43.3 °F | 42.0 °F | 99 % | ESE | 3.1 mph | 7.0 mph | 29.30 in | 0.45 in | 1.88 in |
| 11:34 AM | 43.3 °F | 42.0 °F | 99 % | East | 3.0 mph | 7.0 mph | 29.30 in | 0.45 in | 1.93 in |
| 11:39 AM | 43.3 °F | 42.0 °F | 99 % | East | 3.0 mph | 7.0 mph | 29.28 in | 0.48 in | 2.00 in |
| 11:44 AM | 43.6 °F | 43.5 °F | 99 % | East | 3.5 mph | 7.0 mph | 29.28 in | 0.53 in | 2.06 in |
| 11:49 AM | 43.8 °F | 44.0 °F | 99 % | ESE | 2.2 mph | 7.0 mph | 29.28 in | 0.56 in | 2.16 in |
| 11:54 AM | 44.3 °F | 44.0 °F | 99 % | SSE | 1.3 mph | 6.0 mph | 29.26 in | 0.63 in | 2.24 in |
| 11:59 AM | 45.1 °F | 44.0 °F | 99 % | East | 1.0 mph | 6.0 mph | 29.26 in | 0.71 in | 2.35 in |
| 12:04 PM | 46.1 °F | 46.2 °F | 99 % | NW | 1.4 mph | 6.0 mph | 29.22 in | 0.77 in | 2.42 in |
| 12:09 PM | 49.4 °F | 48.6 °F | 99 % | West | 3.1 mph | 6.0 mph | 29.22 in | 0.85 in | 2.54 in |
| 12:14 PM | 49.5 °F | 48.4 °F | 99 % | ESE | 2.6 mph | 6.0 mph | 29.22 in | 0.88 in | 2.60 in |
| 12:19 PM | 47.6 °F | 46.7 °F | 99 % | East | 1.9 mph | 6.0 mph | 29.22 in | 0.88 in | 2.66 in |
| 12:24 PM | 47.0 °F | 46.0 °F | 99 % | ESE | 1.5 mph | 6.0 mph | 29.22 in | 0.87 in | 2.71 in |
| 12:29 PM | 47.5 °F | 46.8 °F | 99 % | NE | 2.0 mph | 6.0 mph | 29.18 in | 0.86 in | 2.74 in |
| 12:34 PM | 45.9 °F | 45.3 °F | 99 % | ESE | 10.2 mph | 14.3 mph | 29.23 in | 0.98 in | 2.92 in |
| 12:39 PM | 44.5 °F | 44.0 °F | 99 % | ESE | 2.9 mph | 16.0 mph | 29.23 in | 0.99 in | 2.94 in |

**Table 2.** Five minute observations from just south of Catawba, NC. The warm front lifted through this location between 1630-1635 UTC (1130-1135 AM EST).

| Time | Temperature | Dew Point | Humidity | Wind | Speed | Gust | Pressure | Precip. Rate. | Precip. Accum. |
|---|---|---|---|---|---|---|---|---|---|
| 11:00 AM | 44.0 °F | 43.0 °F | 98 % | NE | 1.0 mph | 2.0 mph | 29.53 in | 0.35 in | 2.13 in |
| 11:05 AM | 44.2 °F | 43.0 °F | 98 % | West | 1.0 mph | 2.0 mph | 29.52 in | 0.35 in | 2.14 in |
| 11:10 AM | 45.9 °F | 45.0 °F | 98 % | ENE | 1.0 mph | 3.0 mph | 29.51 in | 0.35 in | 2.17 in |
| 11:15 AM | 48.1 °F | 47.0 °F | 98 % | North | 0.0 mph | 4.0 mph | 29.51 in | 0.34 in | 2.19 in |
| 11:20 AM | 48.1 °F | 47.0 °F | 98 % | North | 0.0 mph | 4.0 mph | 29.51 in | 0.34 in | 2.23 in |
| 11:25 AM | 47.6 °F | 47.0 °F | 98 % | North | 0.0 mph | 6.0 mph | 29.50 in | 0.36 in | 2.27 in |
| 11:30 AM | 47.9 °F | 47.0 °F | 98 % | WNW | 2.0 mph | 6.0 mph | 29.49 in | 0.37 in | 2.30 in |
| 11:35 AM | 50.6 °F | 50.0 °F | 98 % | SSE | 1.0 mph | 5.0 mph | 29.48 in | 0.37 in | 2.32 in |
| 11:40 AM | 53.3 °F | 53.0 °F | 99 % | SSE | 4.0 mph | 8.0 mph | 29.47 in | 0.39 in | 2.36 in |
| 11:45 AM | 54.1 °F | 53.0 °F | 99 % | SSW | 5.0 mph | 10.0 mph | 29.45 in | 0.36 in | 2.38 in |
| 11:50 AM | 54.7 °F | 54.0 °F | 99 % | SSE | 8.0 mph | 10.0 mph | 29.44 in | 0.32 in | 2.41 in |
| 11:55 AM | 55.1 °F | 54.0 °F | 99 % | SW | 4.0 mph | 13.0 mph | 29.44 in | 0.31 in | 2.42 in |
| 12:00 PM | 55.4 °F | 55.0 °F | 99 % | SE | 1.0 mph | 13.0 mph | 29.44 in | 0.32 in | 2.45 in |
| 12:05 PM | 55.7 °F | 55.0 °F | 99 % | SSW | 6.0 mph | 13.0 mph | 29.44 in | 0.34 in | 2.48 in |
| 12:10 PM | 55.9 °F | 55.0 °F | 99 % | SW | 1.0 mph | 13.0 mph | 29.42 in | 0.34 in | 2.51 in |
| 12:15 PM | 56.2 °F | 56.0 °F | 99 % | SW | 4.0 mph | 13.0 mph | 29.43 in | 0.37 in | 2.56 in |
| 12:20 PM | 56.6 °F | 56.0 °F | 99 % | SSE | 5.0 mph | 10.0 mph | 29.41 in | 0.39 in | 2.63 in |
| 12:25 PM | 56.7 °F | 56.0 °F | 99 % | South | 2.0 mph | 16.0 mph | 29.39 in | 0.40 in | 2.68 in |
| 12:30 PM | 56.9 °F | 56.0 °F | 99 % | South | 11.0 mph | 16.0 mph | 29.39 in | 0.42 in | 2.72 in |
| 12:35 PM | 49.7 °F | 49.0 °F | 98 % | NW | 8.0 mph | 26.0 mph | 29.49 in | 0.59 in | 2.91 in |
| 12:40 PM | 47.1 °F | 45.0 °F | 95 % | SW | 5.0 mph | 26.0 mph | 29.49 in | 0.69 in | 3.05 in |

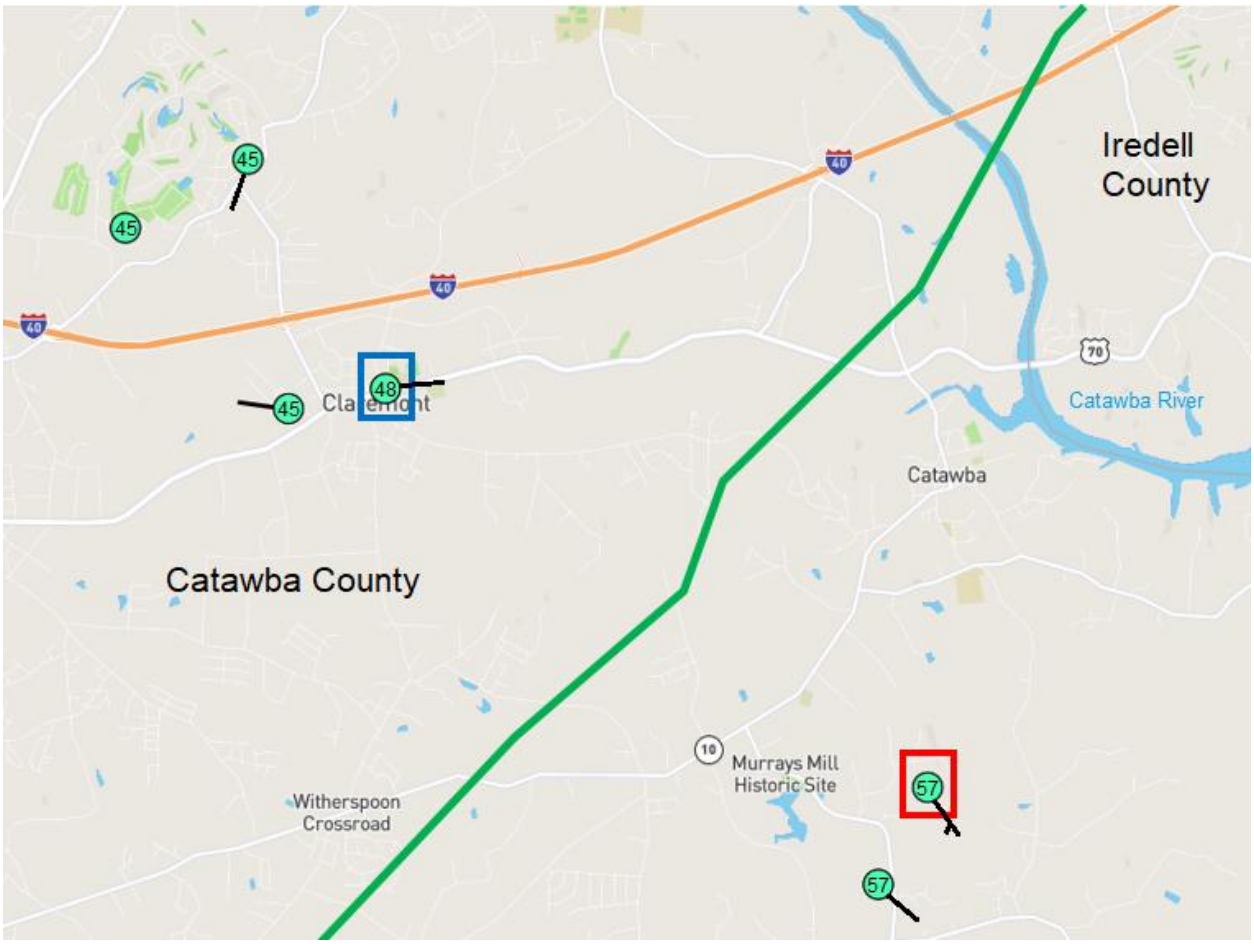


**Fig. 18.** Temperature (°F) and wind (mph) from Weather Underground stations from 1715 UTC to 1720 UTC 9 January (observation time closest to the beginning time of the Claremont Tornado). The location of the Claremont weather station on the cool side of the warm front is shown by the blue box and the Catawba weather station on the warm side of the front is shown in the red box. The tornado track (green line) is also overlaid.

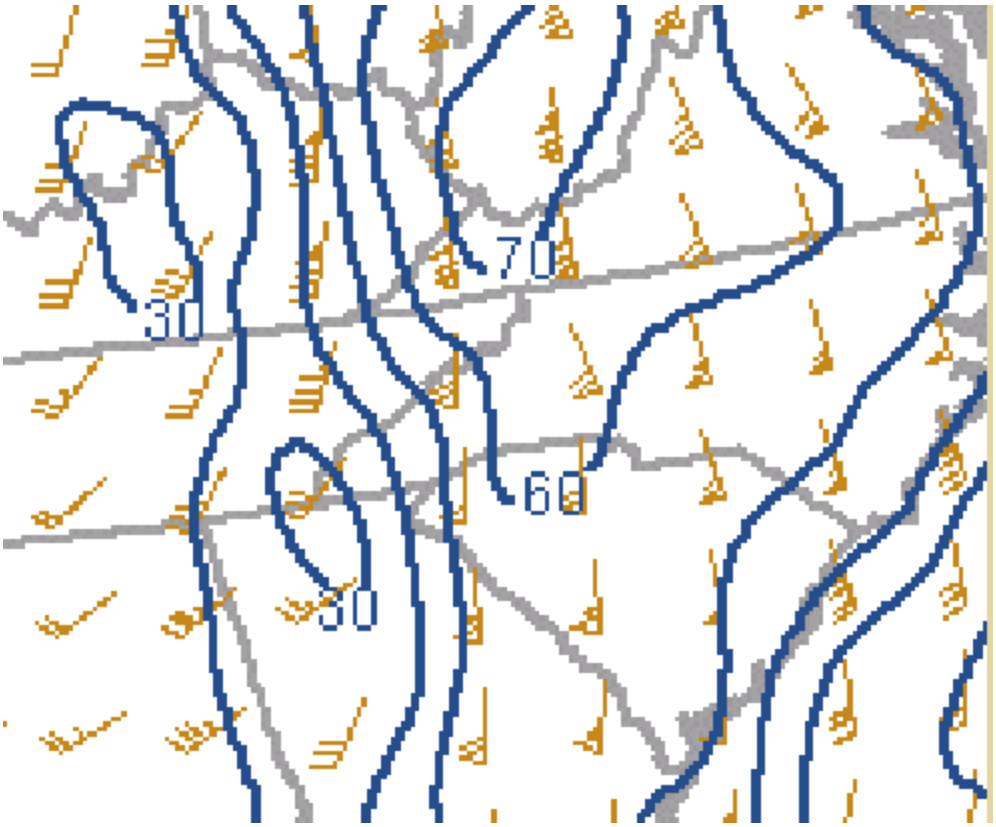


**Fig. 19.** SPC objective analysis of surface-to-1 km bulk shear (kt; dark blue contours) and shear vector (barbs) at 1700 UTC 9 January.

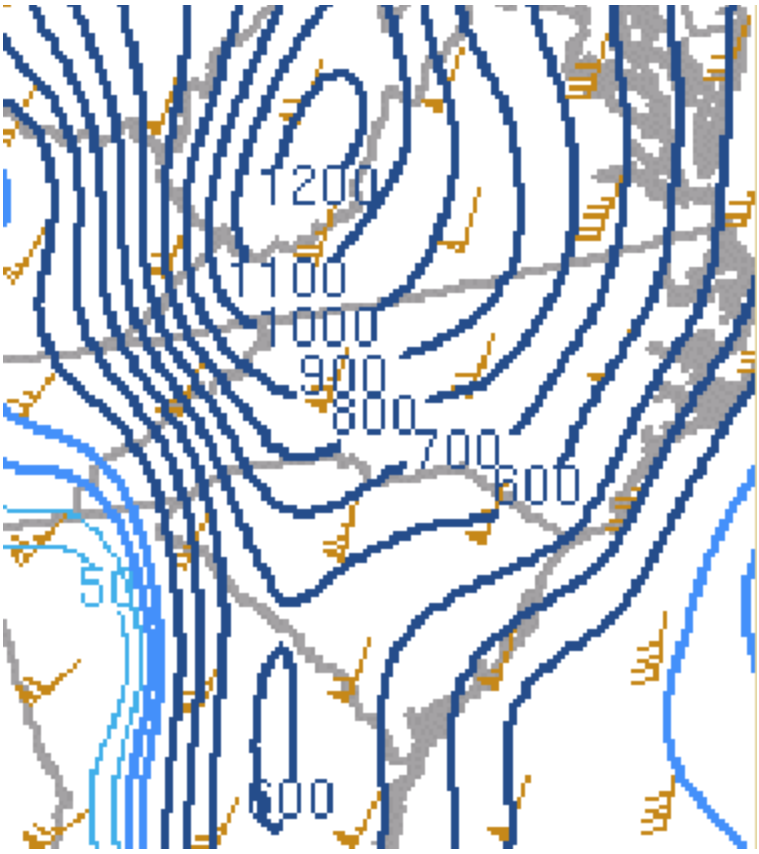


**Fig. 20.** SPC objective analysis of surface-to-1 km SRH ($m^2 s^{-2}$; dark blue and light blue contours) and storm motion (kt; barbs) at 1700 UTC 9 January.

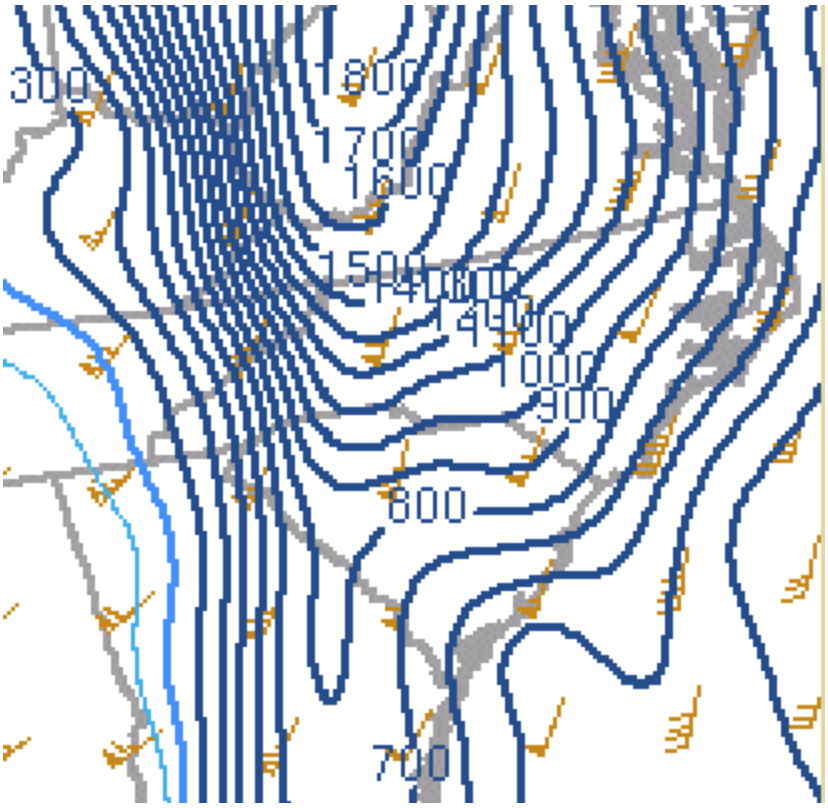


**Fig. 21.** SPC objective analysis of surface-to-3 km SRH ($m^2 s^{-2}$; dark blue and light blue contours) and storm motion (kt; barbs) at 1700 UTC 9 January.

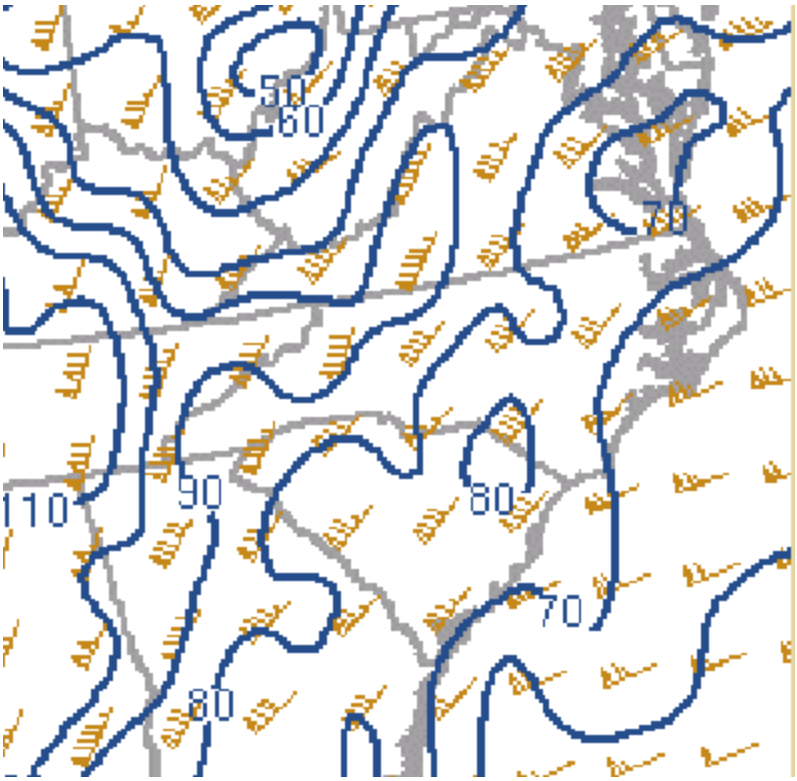


**Fig. 22.** SPC objective analysis of surface-to-6 km bulk shear (kts; dark blue contours) and shear vector (barbs) at 1700 UTC 9 January.

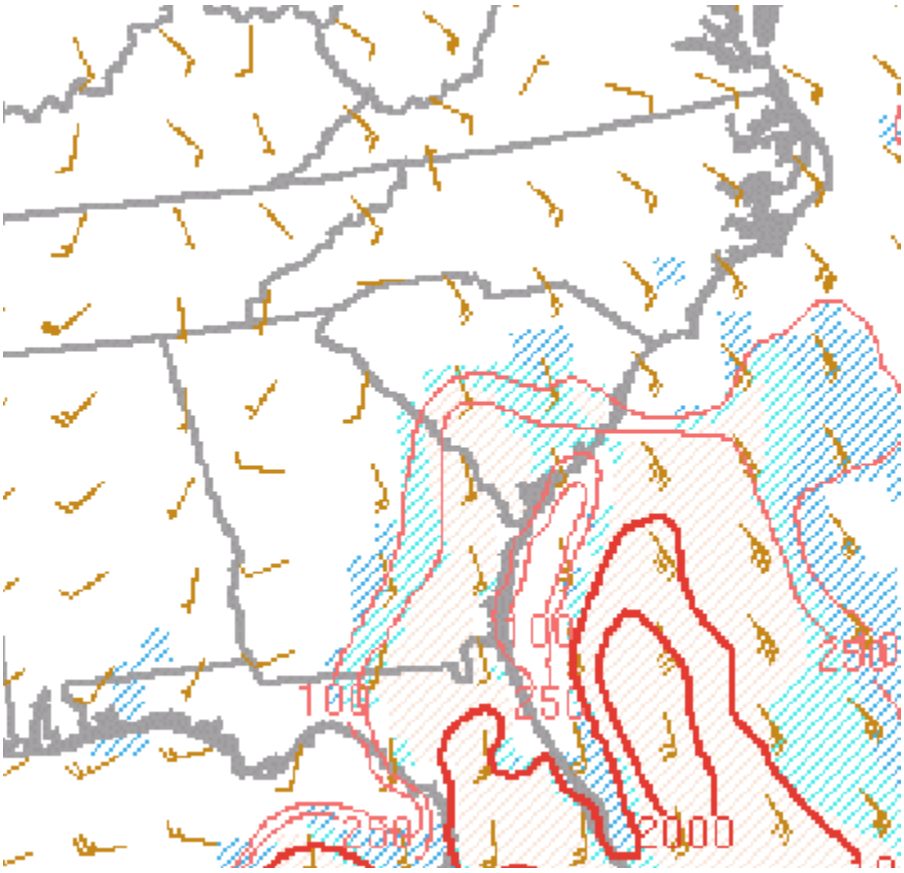

**Fig. 23.** SPC objective analysis of SBCAPE (J kg$^{-1}$; red contours) and surface-based convective inhibition (SBCIN, J kg$^{-1}$; cross hatching) at 1700 UTC 9 January.

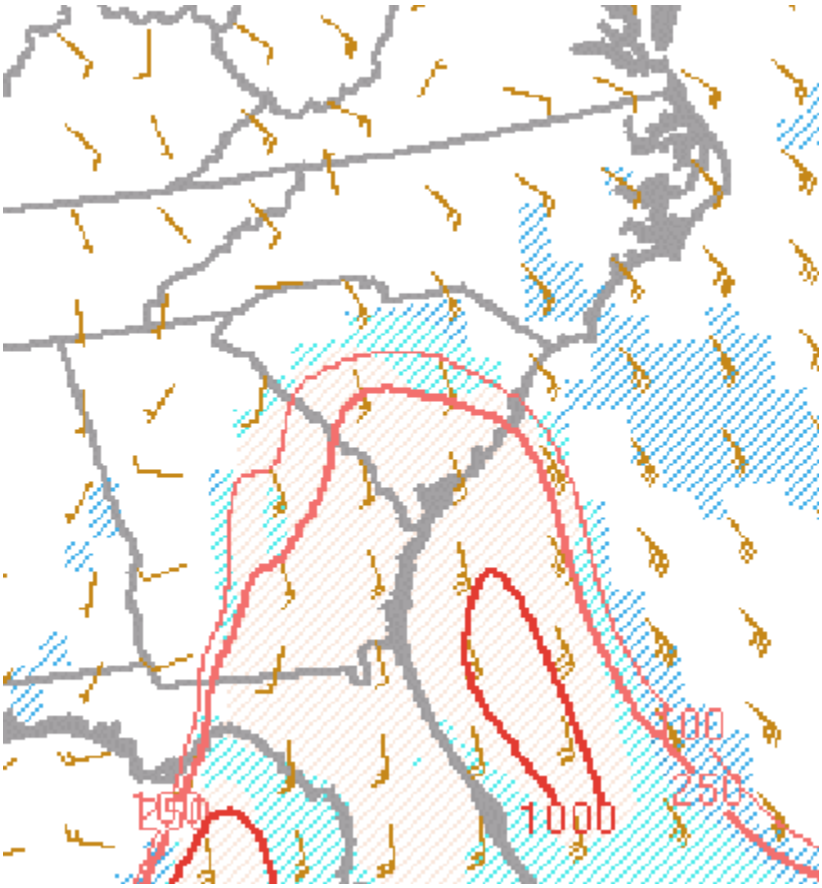


**Fig. 24.** SPC objective analysis of MLCAPE (J kg$^{-1}$; red contours) and SBCIN (J kg$^{-1}$; cross hatching) at 1700 UTC 9 January.

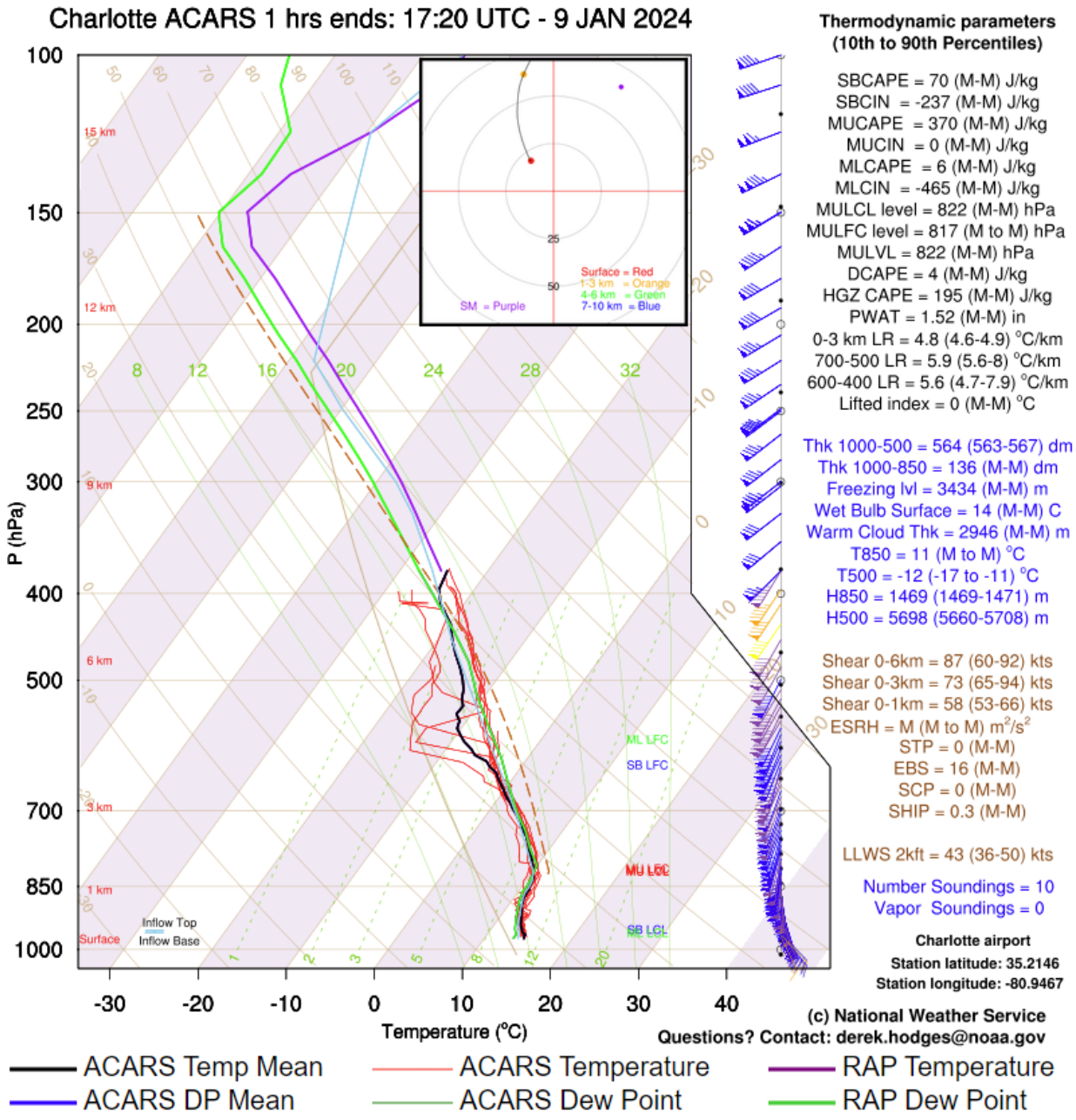


**Fig. 25.** ACARS sounding at KCLT at 1720 UTC on 9 January.

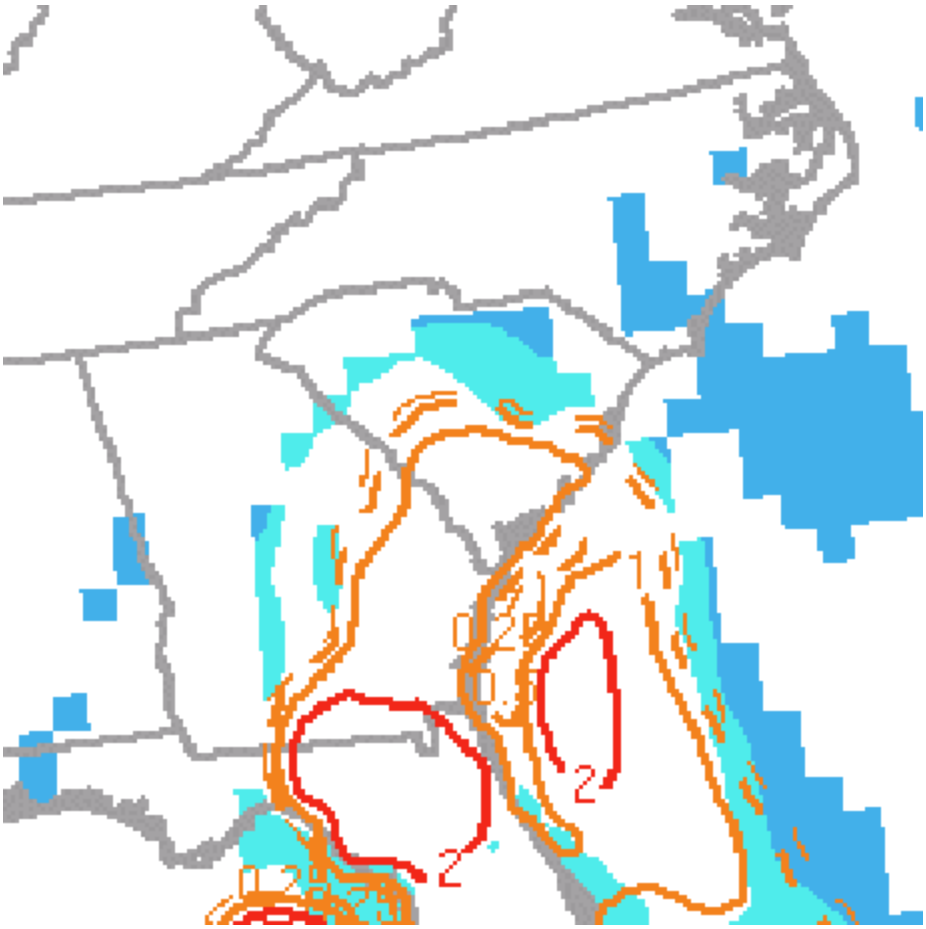


**Fig. 26.** SPC objective analysis of STP (red and orange contours) and SBCIN (J $kg^{-1}$; color fill) at 1700 UTC 9 January.

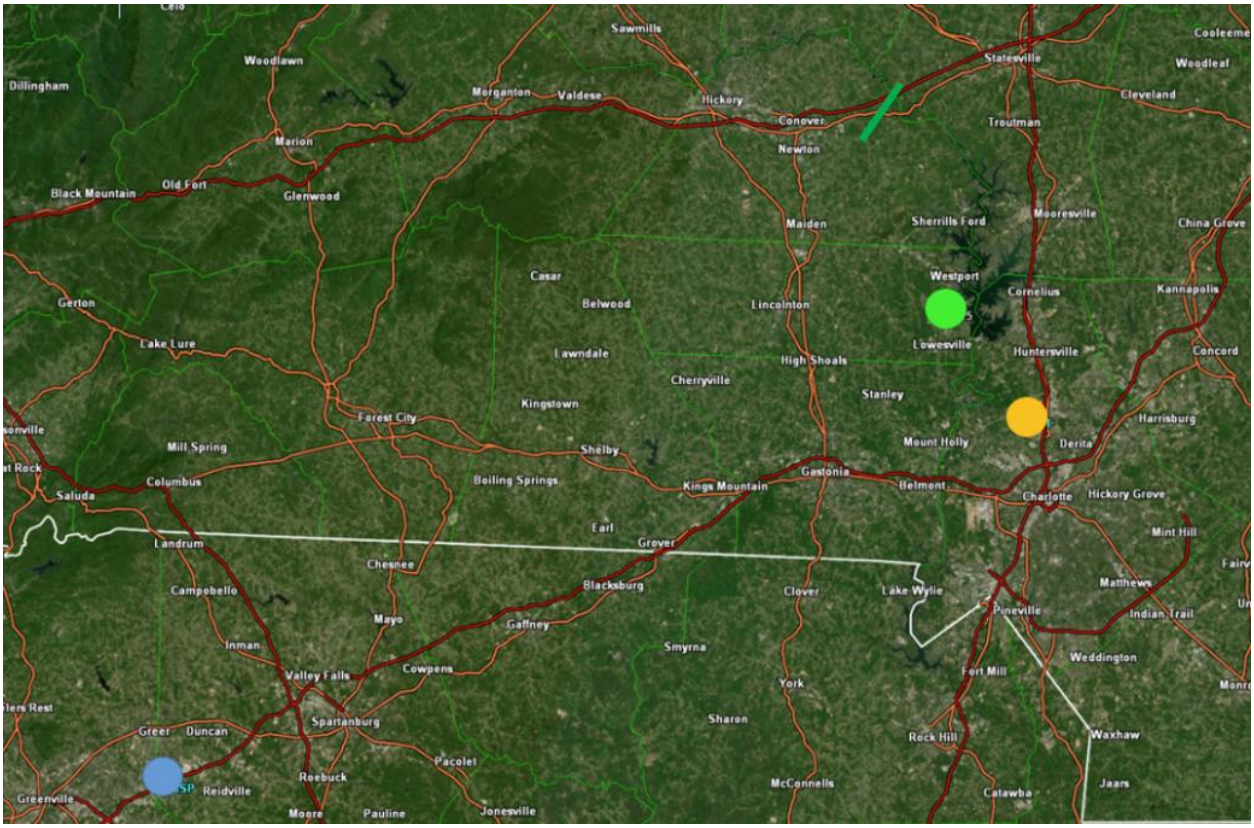


**Fig. 27.** Location of KGSP (blue circle), TCLT (orange circle), and V025 (green circle) in relation to the tornado track (green line).

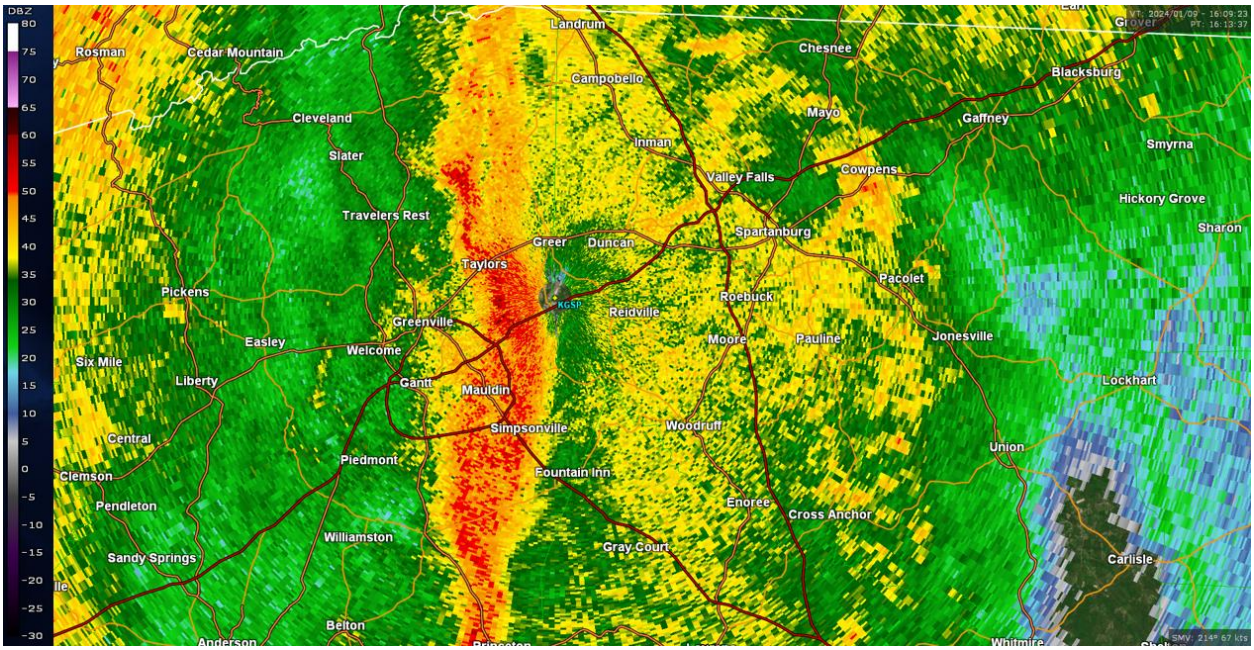


**Fig. 28.** Base reflectivity (dBZ; 1.8° scan) from KGSP at 1613 UTC.

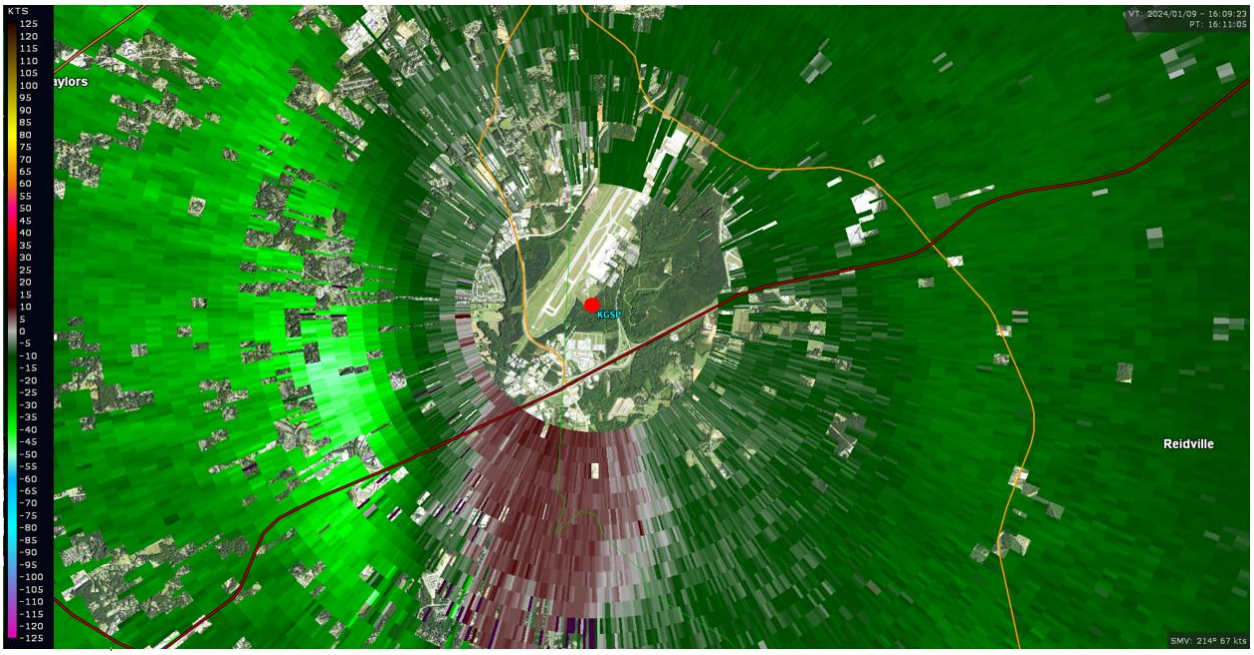


**Fig. 29.** Base velocity (kts; 0.2° scan) from KGSP (red dot) at 1611 UTC with 50 kts at 56 ft ARL approaching the radar.

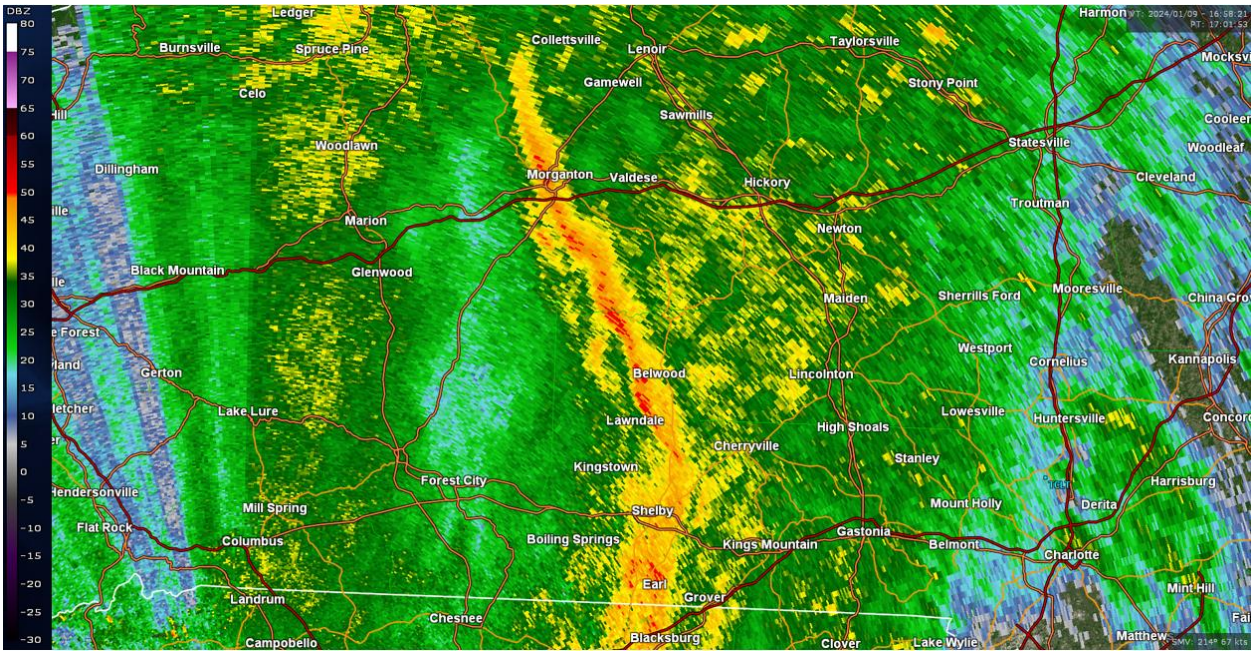


**Fig. 30.** Base reflectivity (dBZ; 0.2° scan) from KGSP at 1701 UTC.

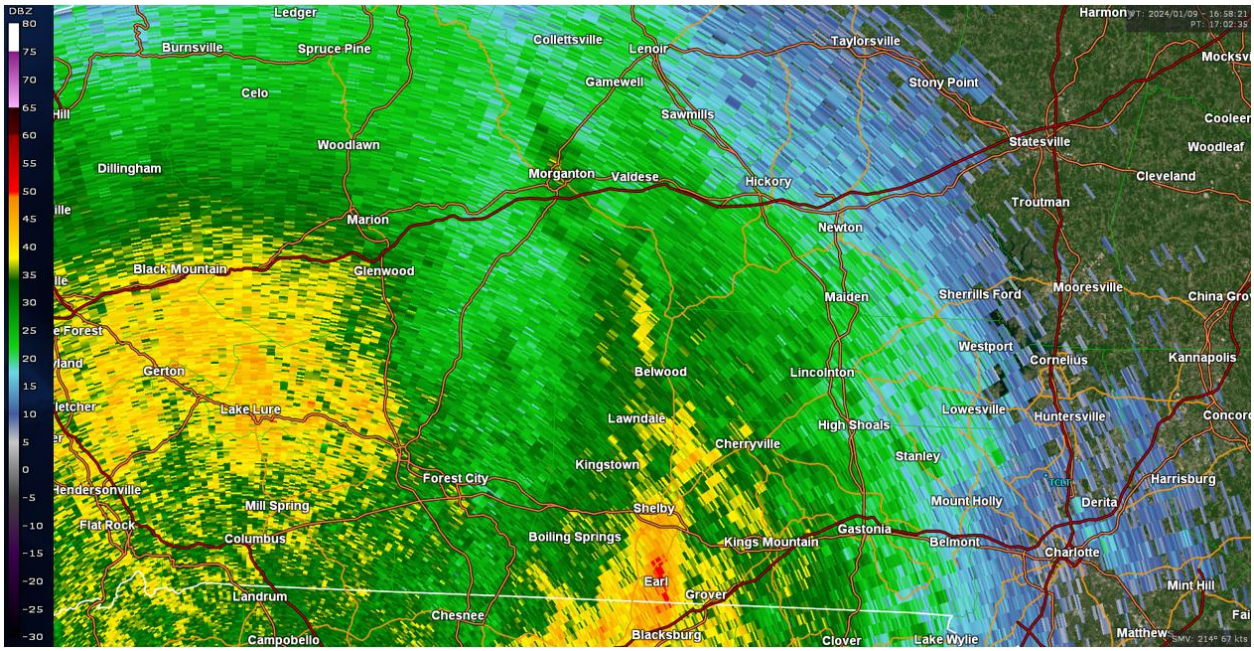


**Fig. 31.** As in Fig. 30, but at the 1.8° elevation tilt.

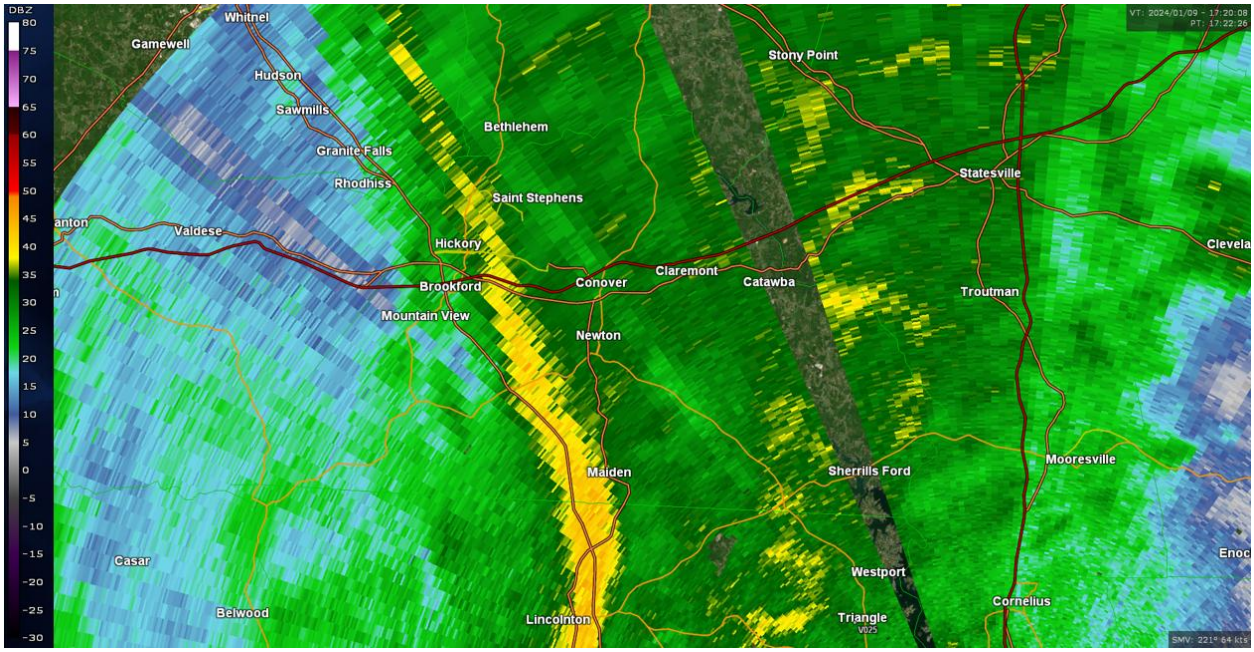


**Fig. 32.** Base reflectivity (dBZ; 0.2° scan) from TCLT at 1722 UTC.

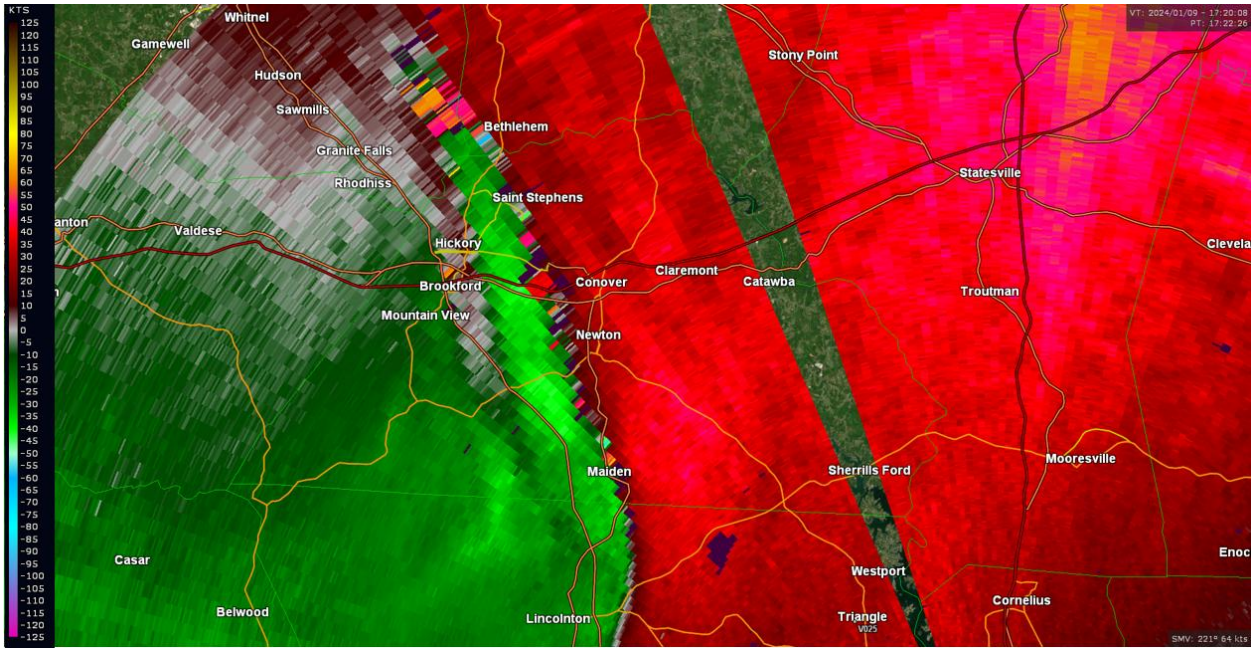


**Fig. 33.** As in Fig. 32, but for base velocity (kts).

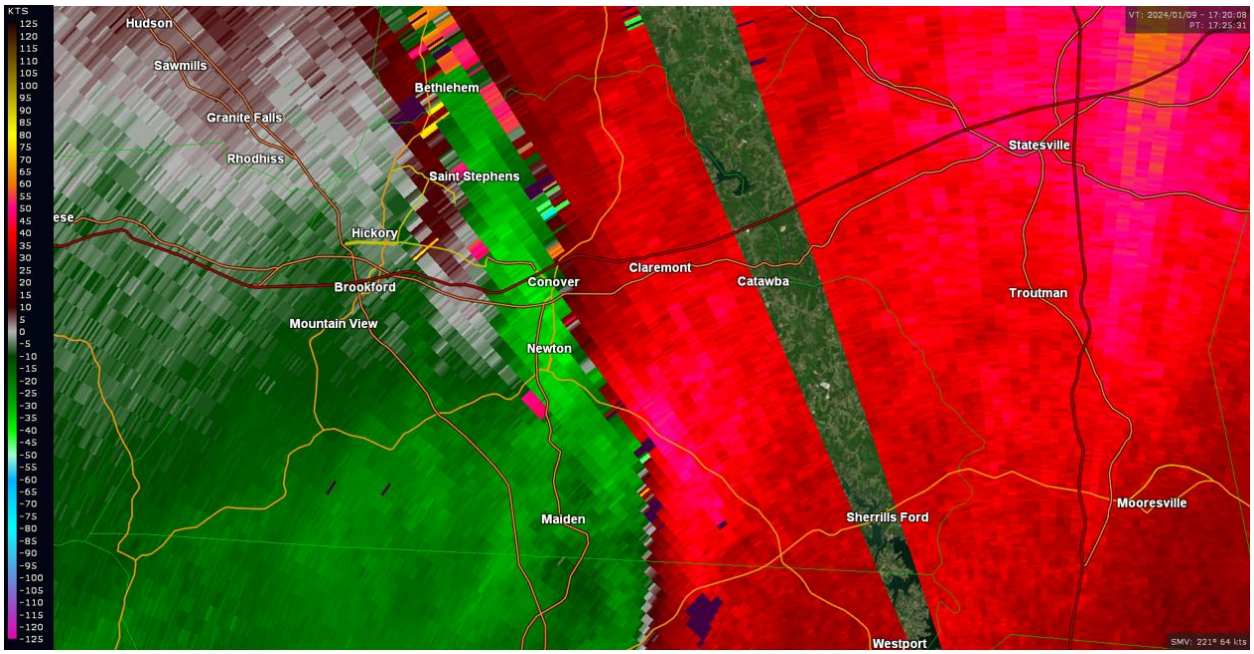


**Fig. 34.** Base velocity (kts; 0.2° scan) from TCLT at 1725 UTC.

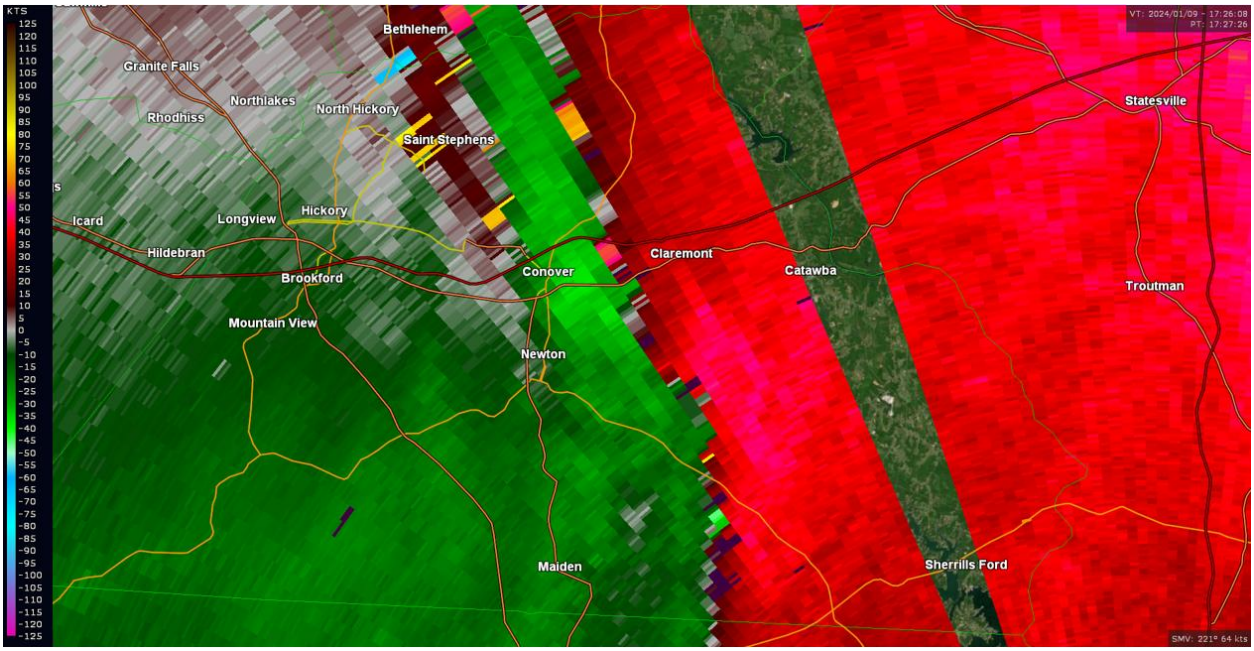


**Fig. 35.** As in Fig. 34, but at 1727 UTC.

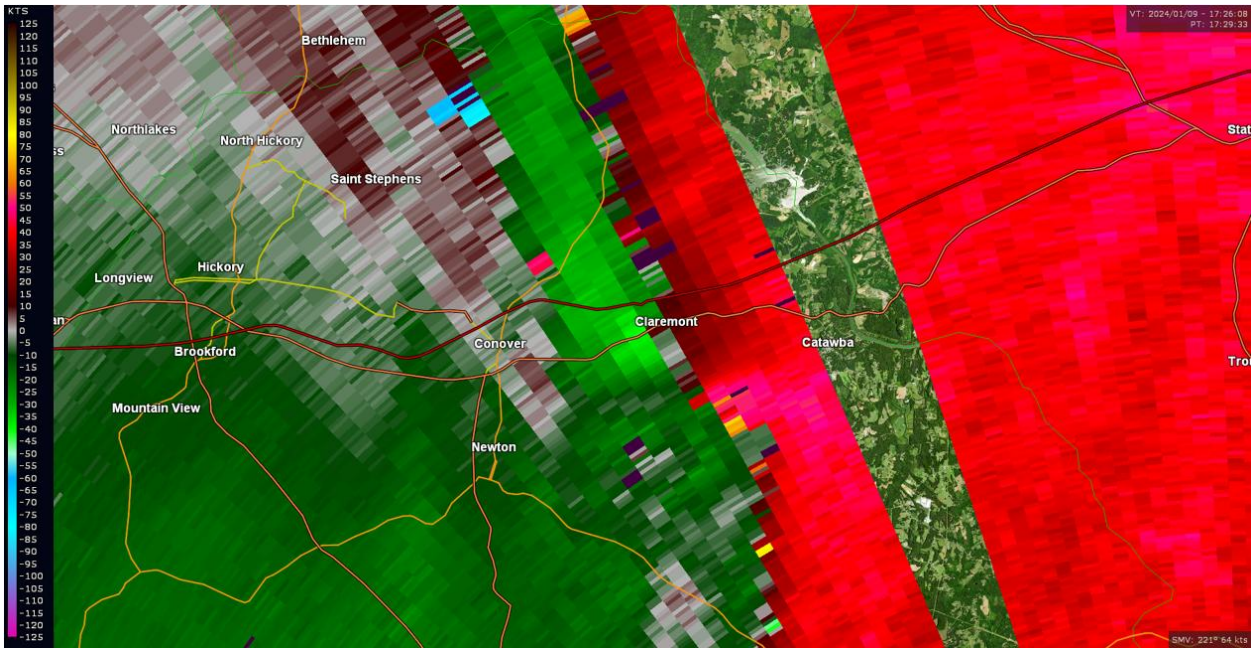


**Fig. 36.** As in Fig. 34, but at 1729 UTC.

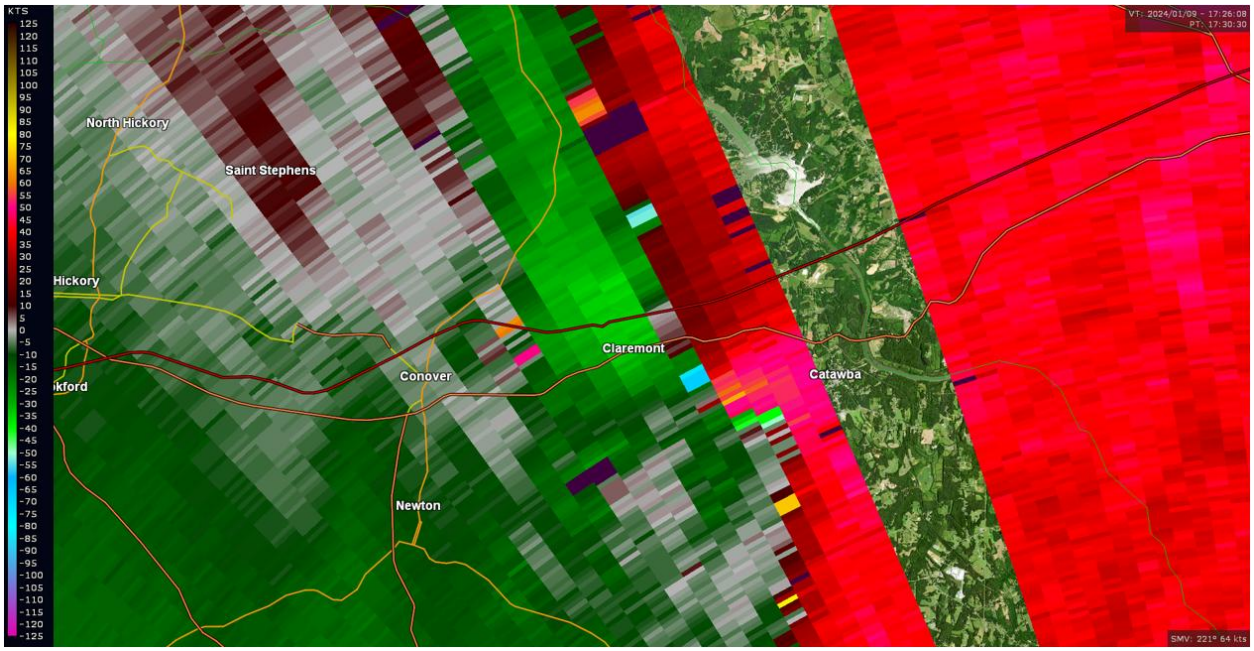


**Fig. 37.** As in Fig. 34, but at 1730 UTC.

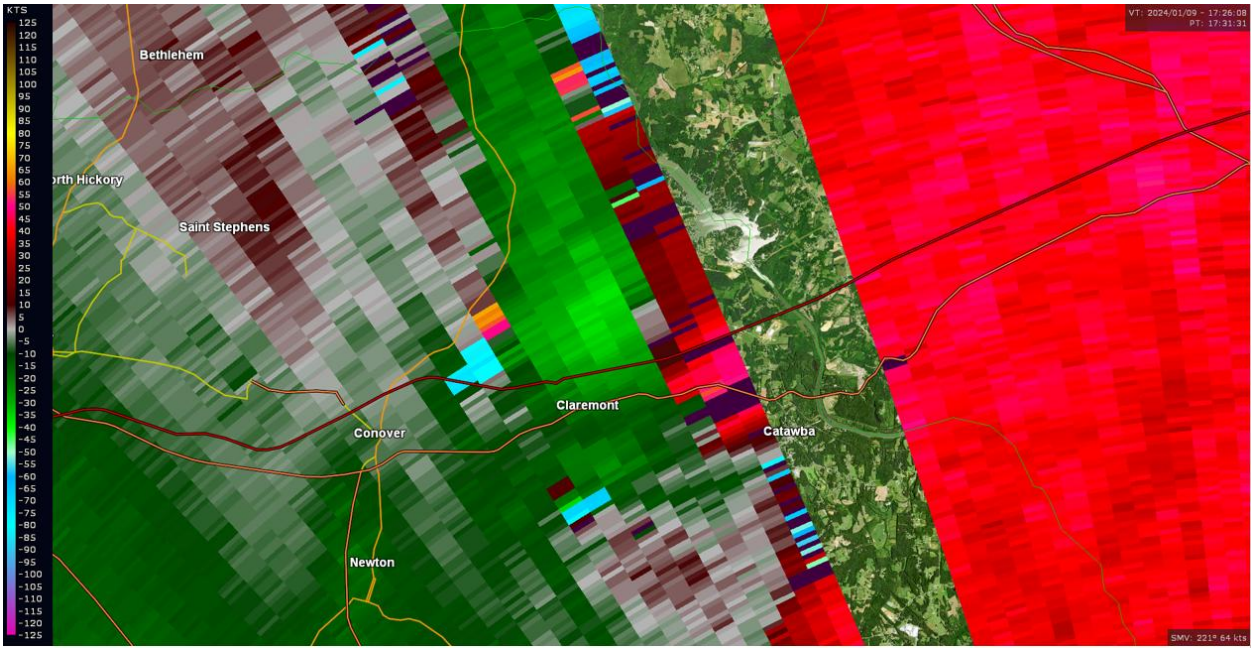


**Fig. 38.** As in Fig. 34, but at 1731 UTC.

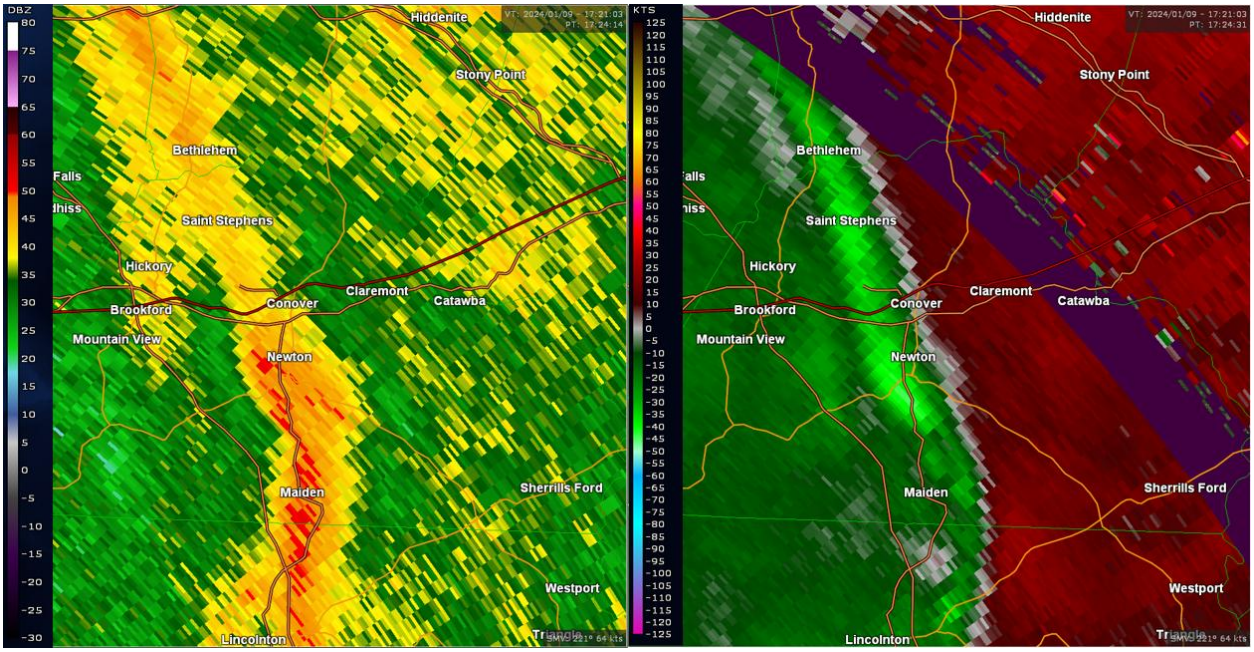


**Fig. 39.** Base reflectivity (dBZ; 0.2° scan) (left) and SRV (kts; 0.2° scan) (right) from KGSP at 1724 UTC.

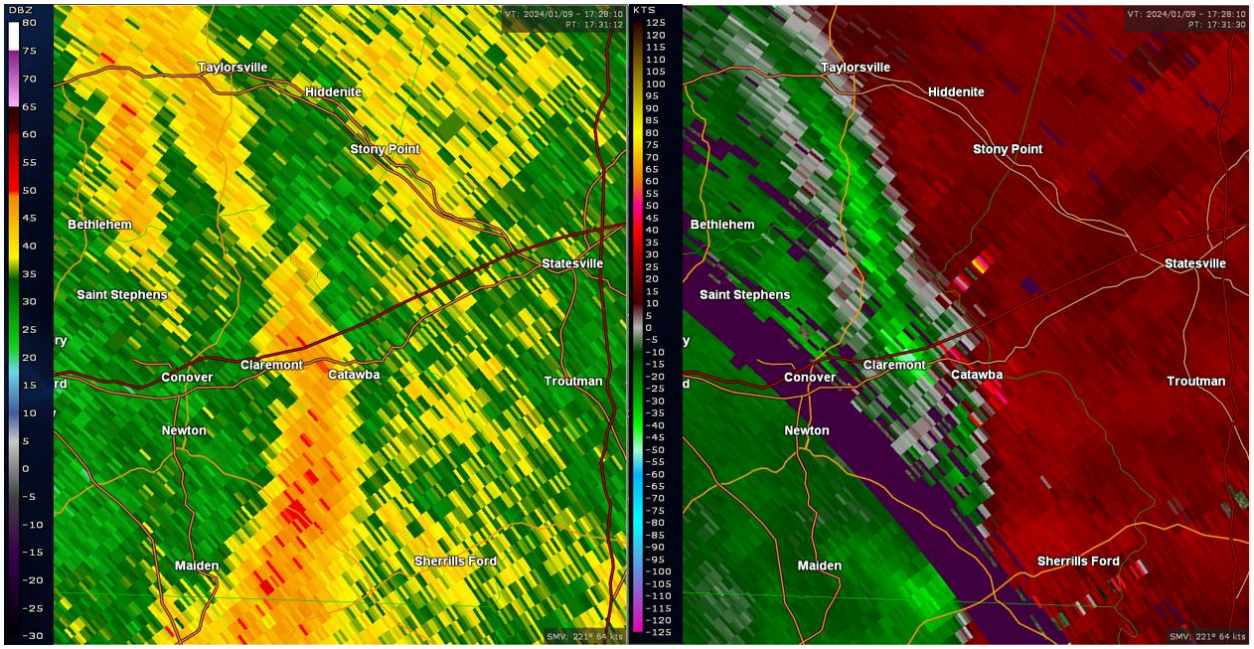


**Fig. 40.** As in Fig. 39, but at 1731 UTC.

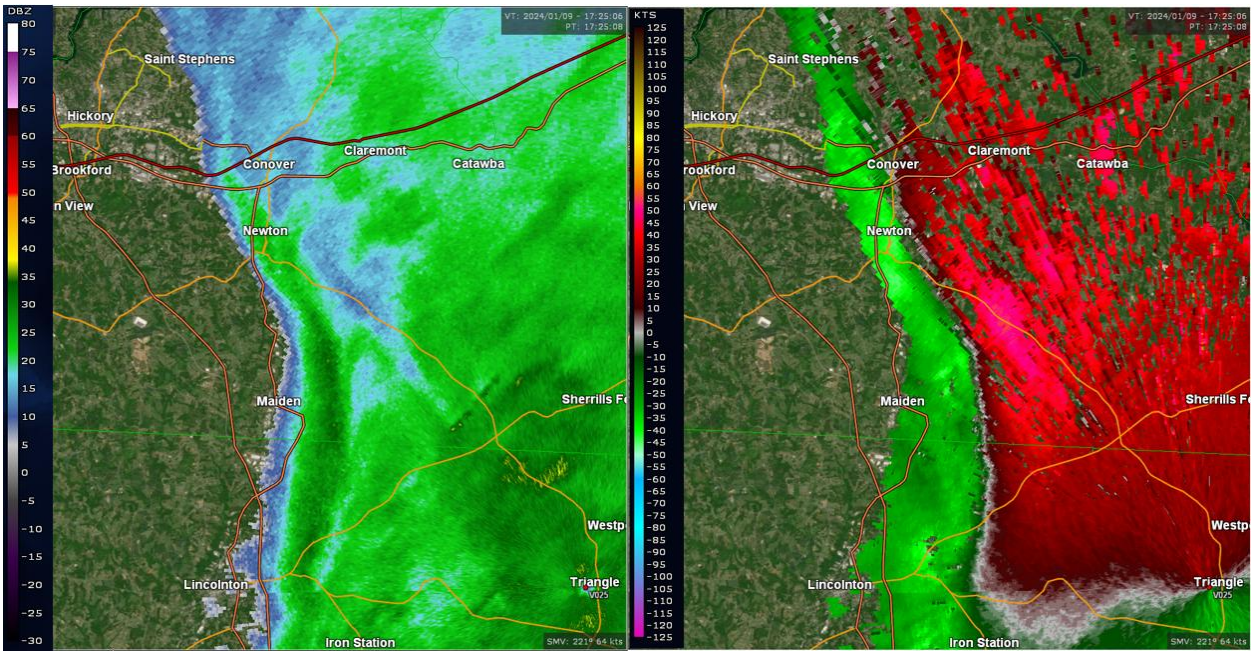


**Fig. 41.** Base reflectivity (dBz; 0.5° scan) (left) and velocity (kts; 0.5° scan) (right) from V025 at 1725 UTC.

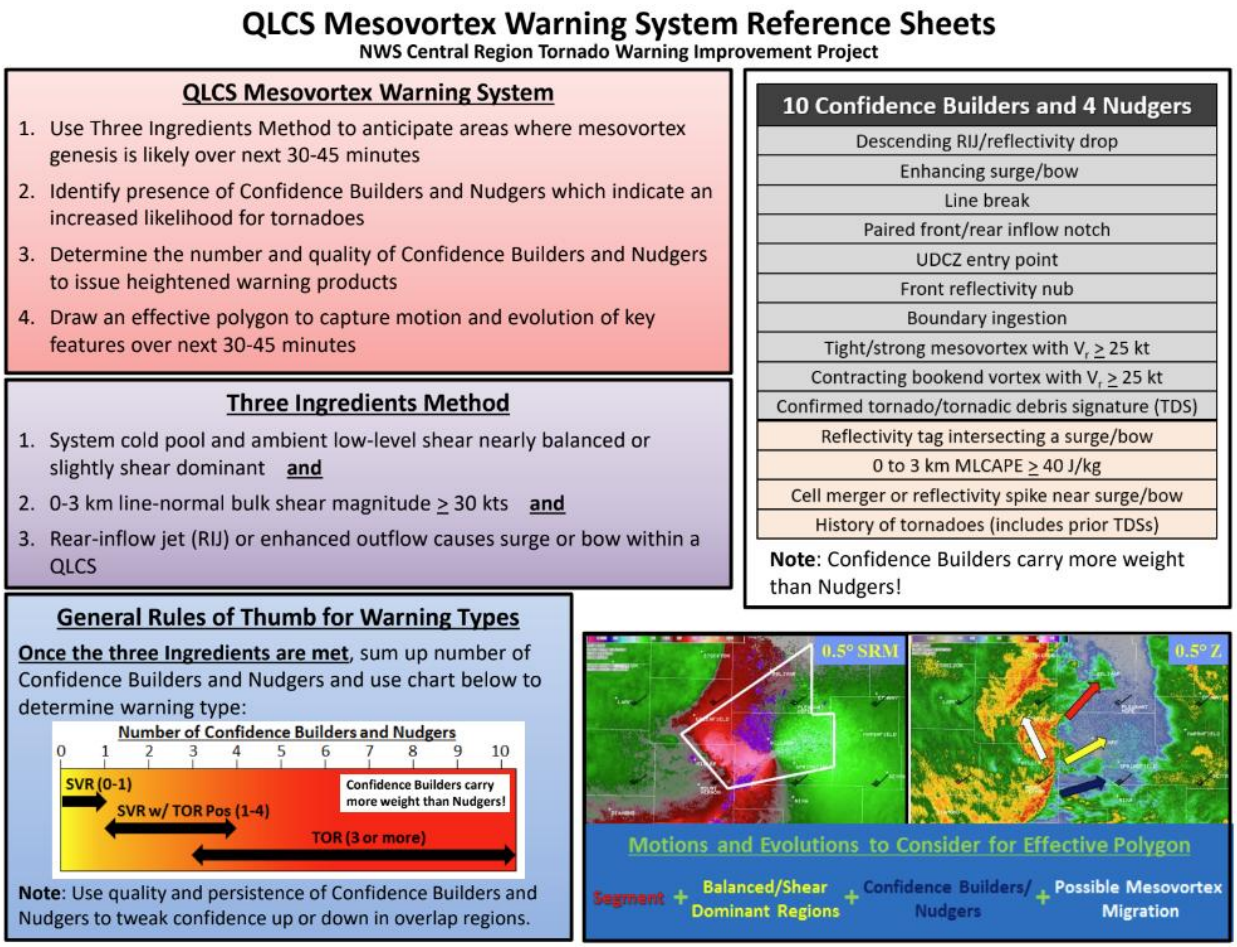


**Fig. 42.** QLCS Mesovortex Warning System reference (NWS Central Region Tornado Warning Improvement Project).

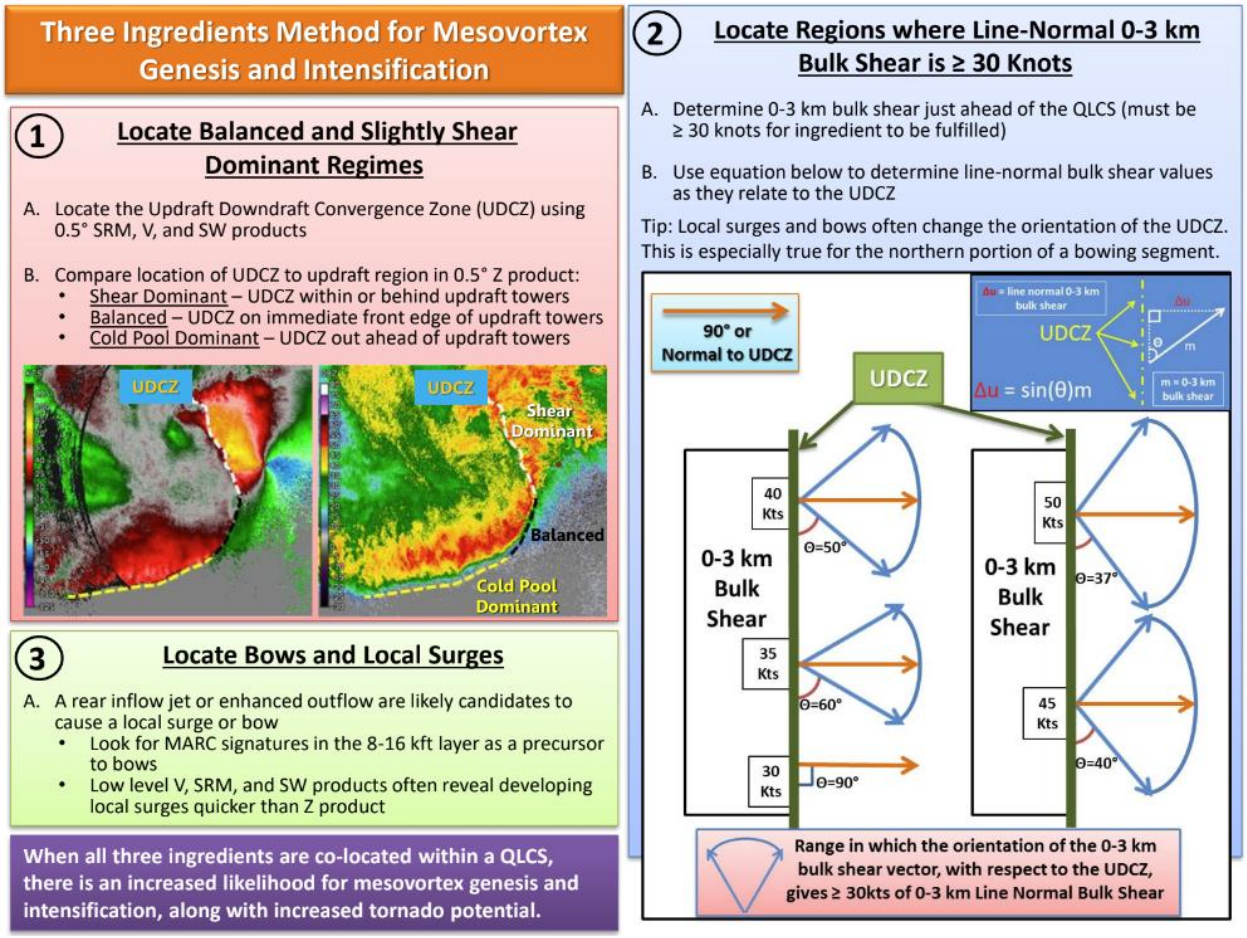


**Fig. 43.** Three Ingredients Method as part of the QLCS Mesovortex Warning System (NWS Central Region Tornado Warning Improvement Project).

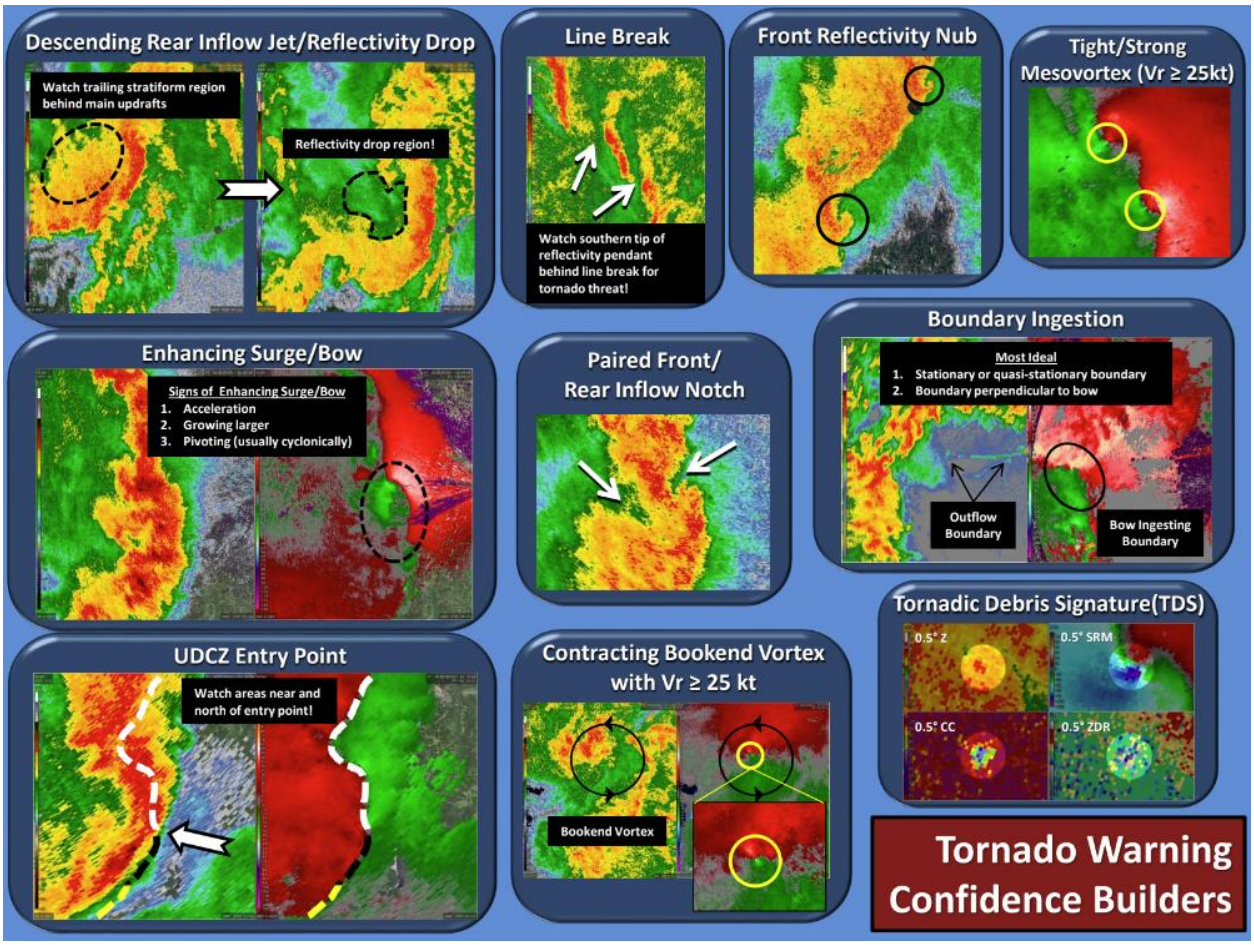


**Fig. 44.** Common confidence building radar signatures commonly associated with QLCS tornadoes as part of the QLCS Mesovortex Warning System (NWS Central Region Tornado Warning Improvement Project).

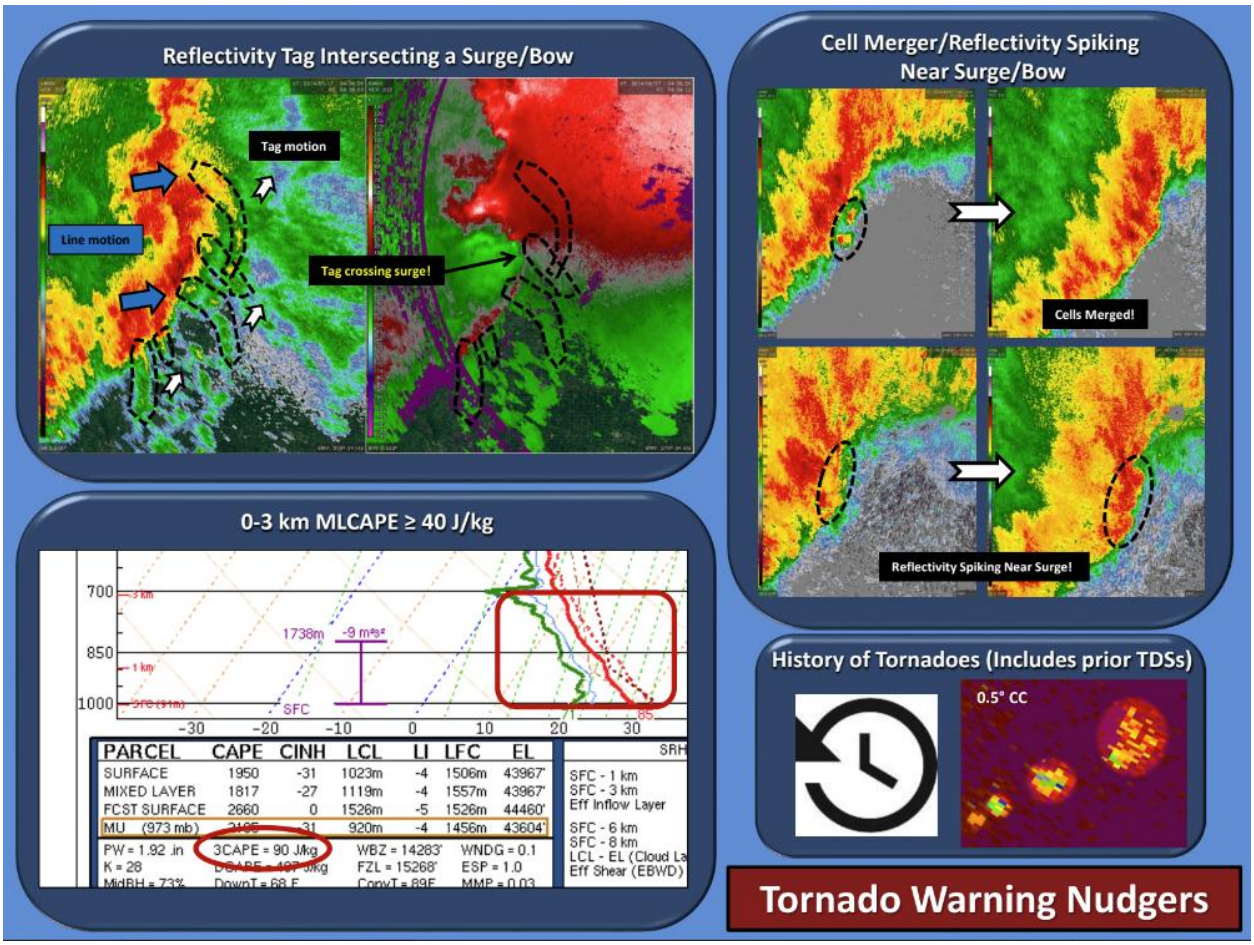


**Fig. 45.** Tornado warning nudgers used in the QLCS Mesovortex Warning System (NWS Central Region Tornado Warning Improvement Project).

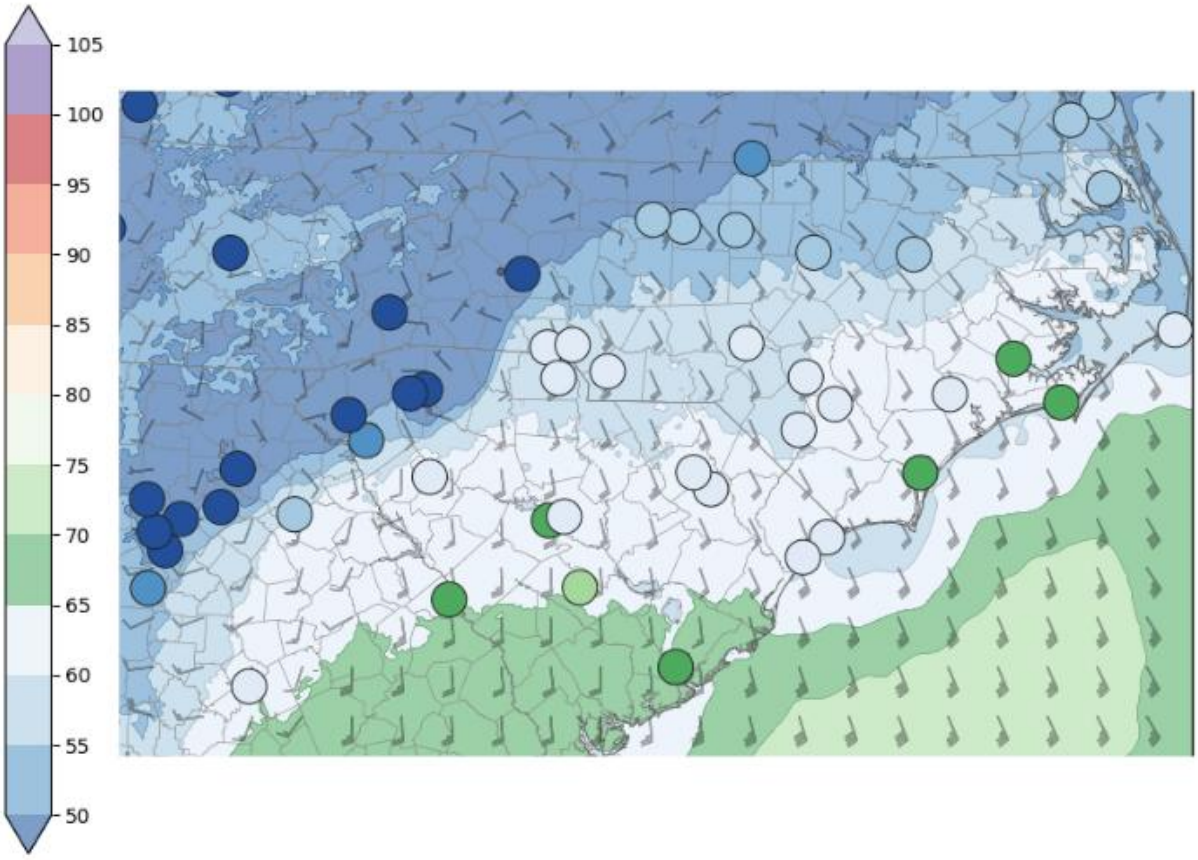


**Fig. 46.** WoFS mean 2 m temperature (°F; image), ASOS observed temperature (°F; color-filled dots) and 10 m wind (barbs) valid at 1700 UTC.

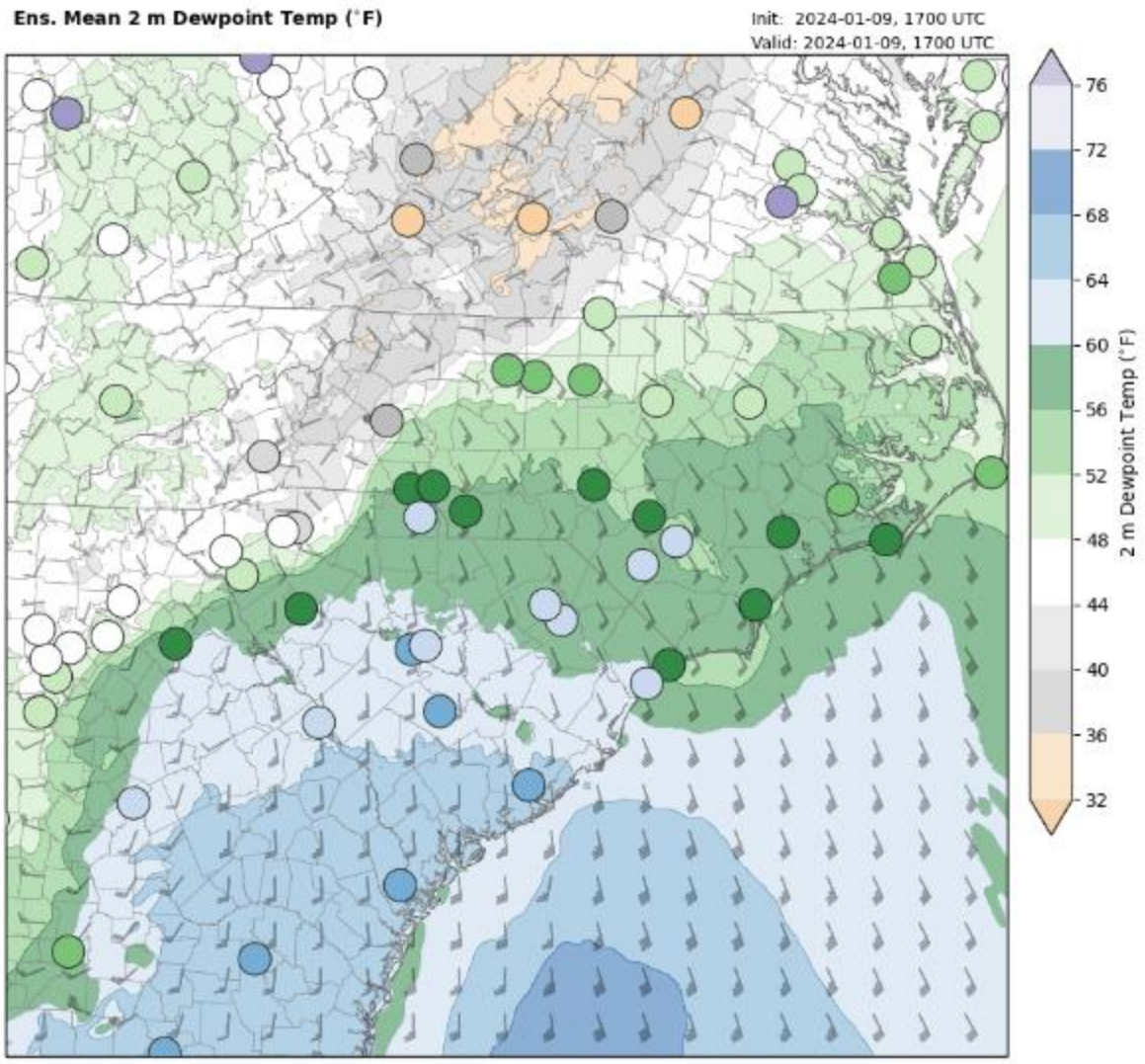


**Fig. 47.** As in Fig. 46, but for 2 m dewpoint (°F).

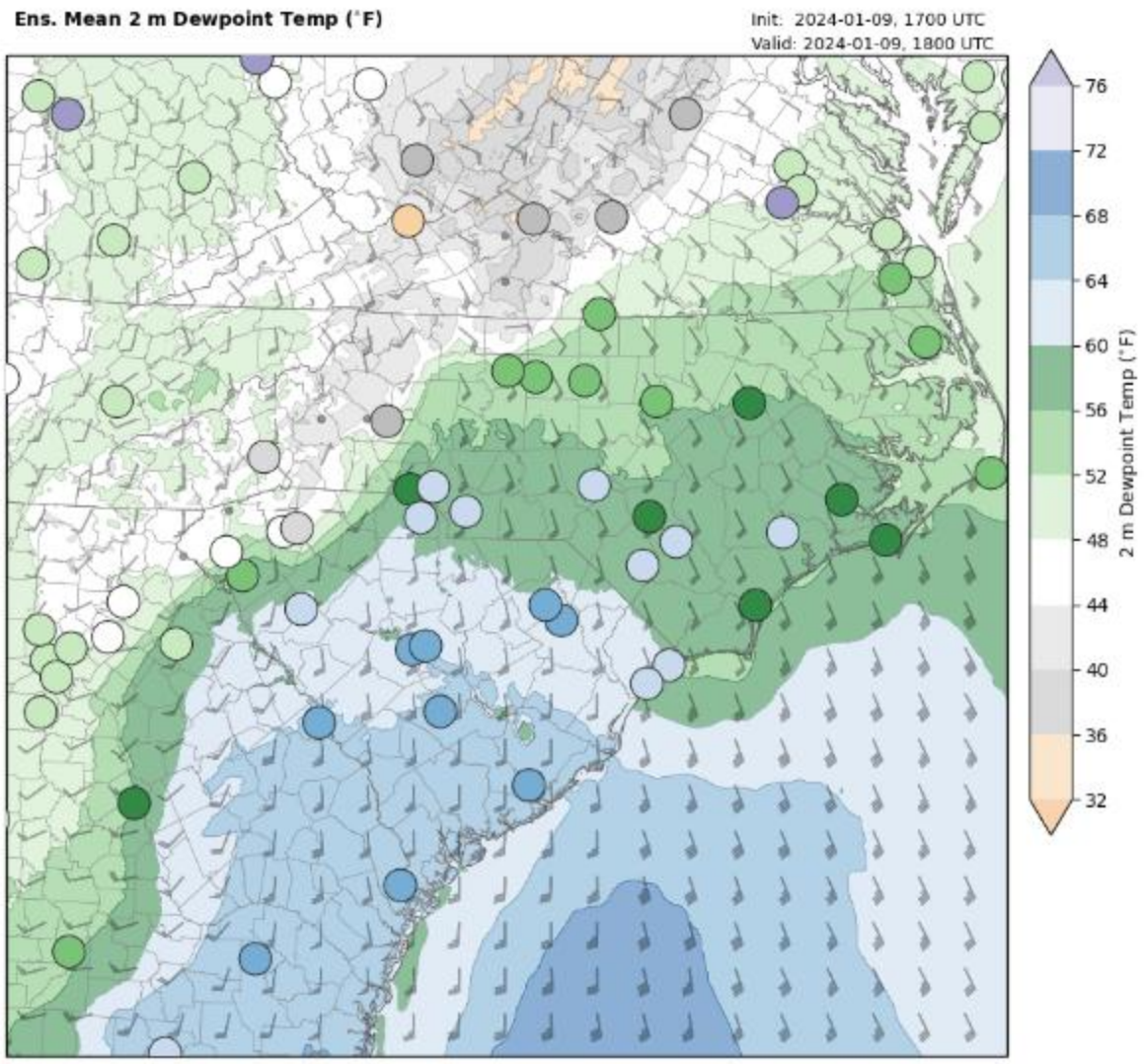


**Fig. 48.** As in Fig. 47, but at 1800 UTC.

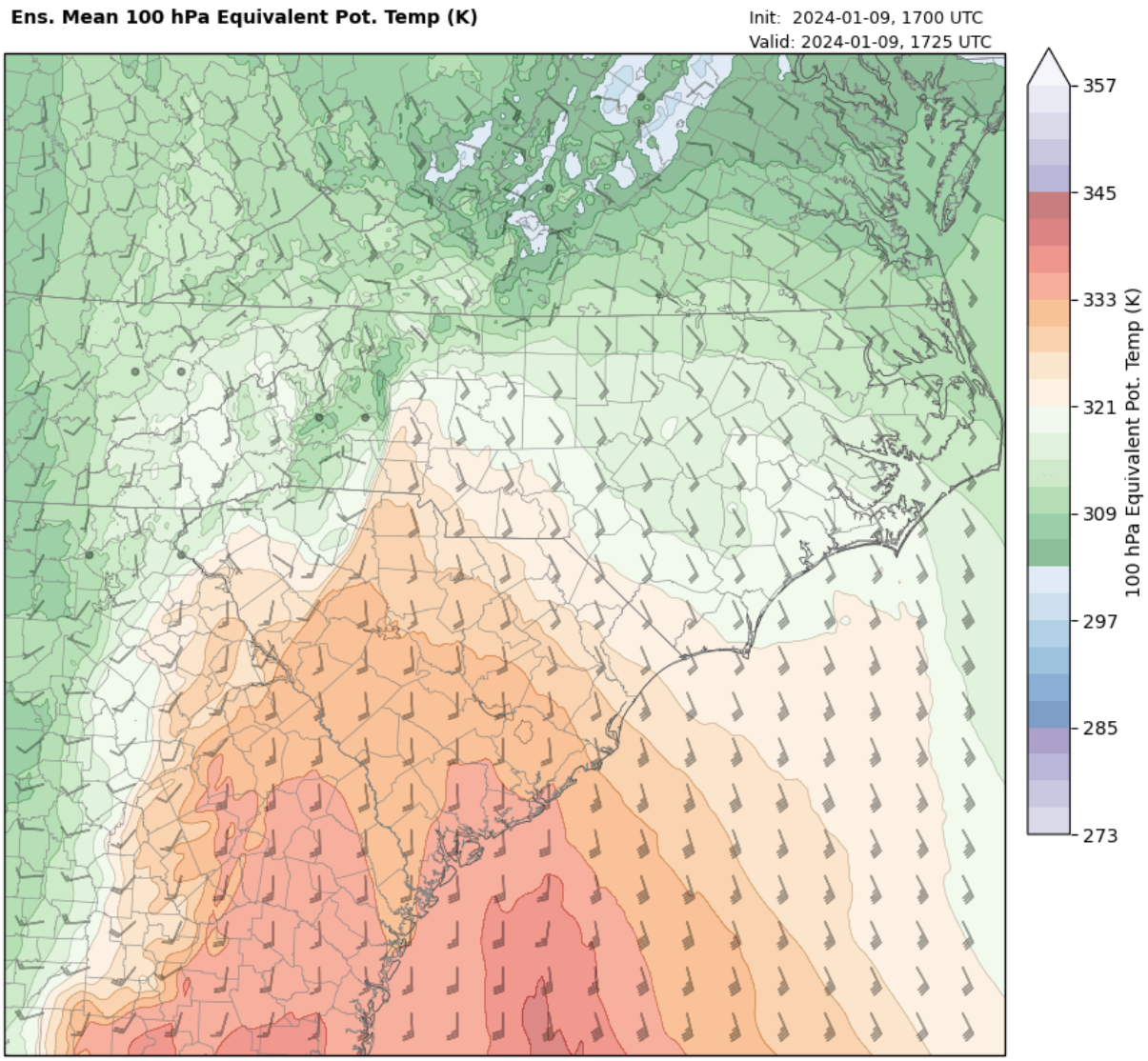


**Fig. 49.** WoFS mean lowest 100 mb equivalent potential temperature (K; color fill) and 10 m wind (barbs) valid at 1725 UTC.

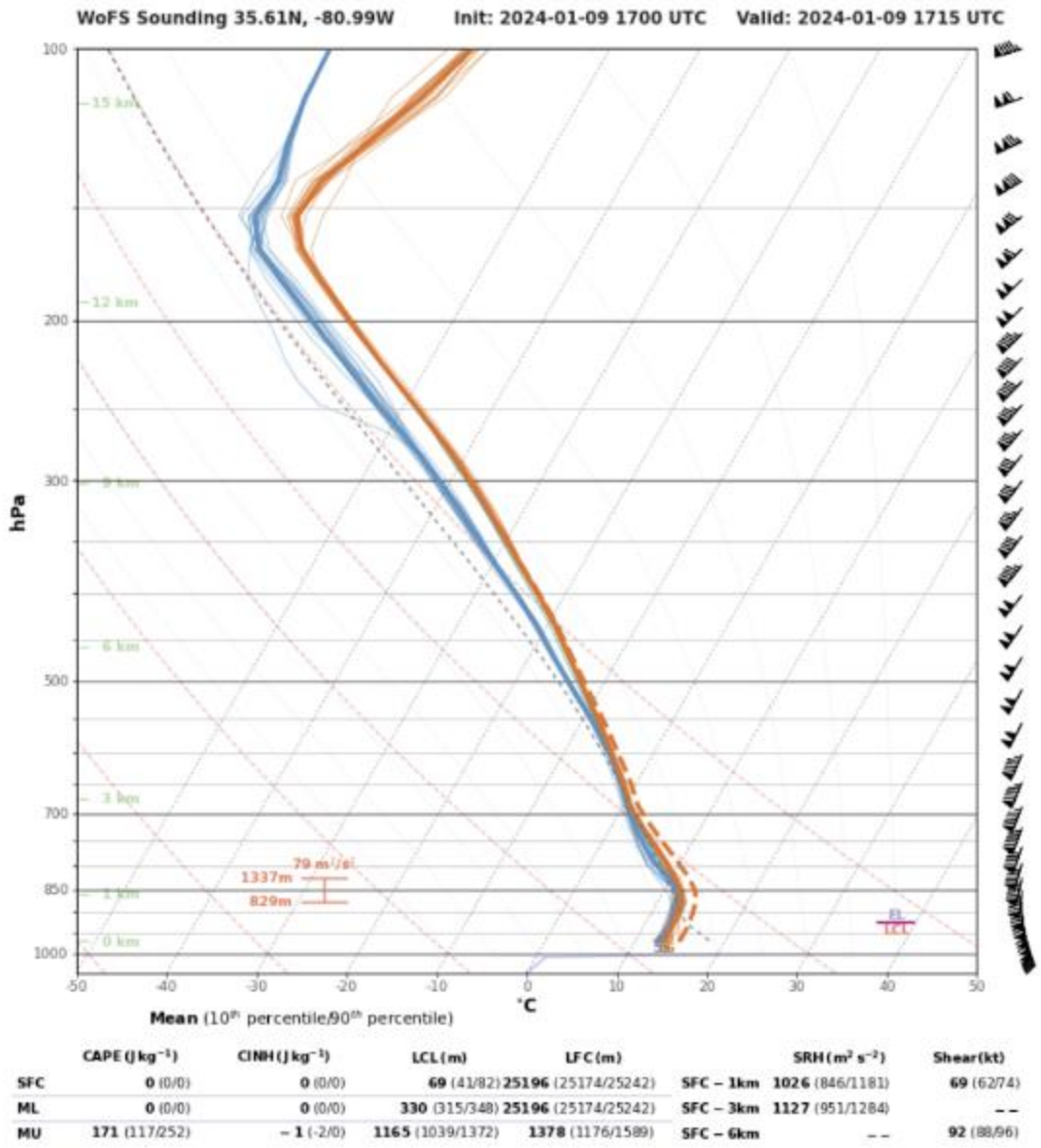


| | CAPE (J kg$^{-1}$) | CINH (J kg$^{-1}$) | LCL (m) | LFC (m) | | SRH (m$^2$ s$^{-2}$) | Shear (kt) |
|---|---|---|---|---|---|---|---|
| SFC | **0** (0/0) | **0** (0/0) | **69** (41/82) | **25196** (25174/25242) | SFC – 1km | **1026** (846/1181) | **69** (62/74) |
| ML | **0** (0/0) | **0** (0/0) | **330** (315/348) | **25196** (25174/25242) | SFC – 3km | **1127** (951/1284) | – – |
| MU | **171** (117/252) | **– 1** (-2/0) | **1165** (1039/1372) | **1378** (1176/1589) | SFC – 6km | – – | **92** (88/96) |

**Fig. 50.** WoFS forecast sounding valid at 1715 UTC at a location 12 miles southeast of the Claremont Tornado.

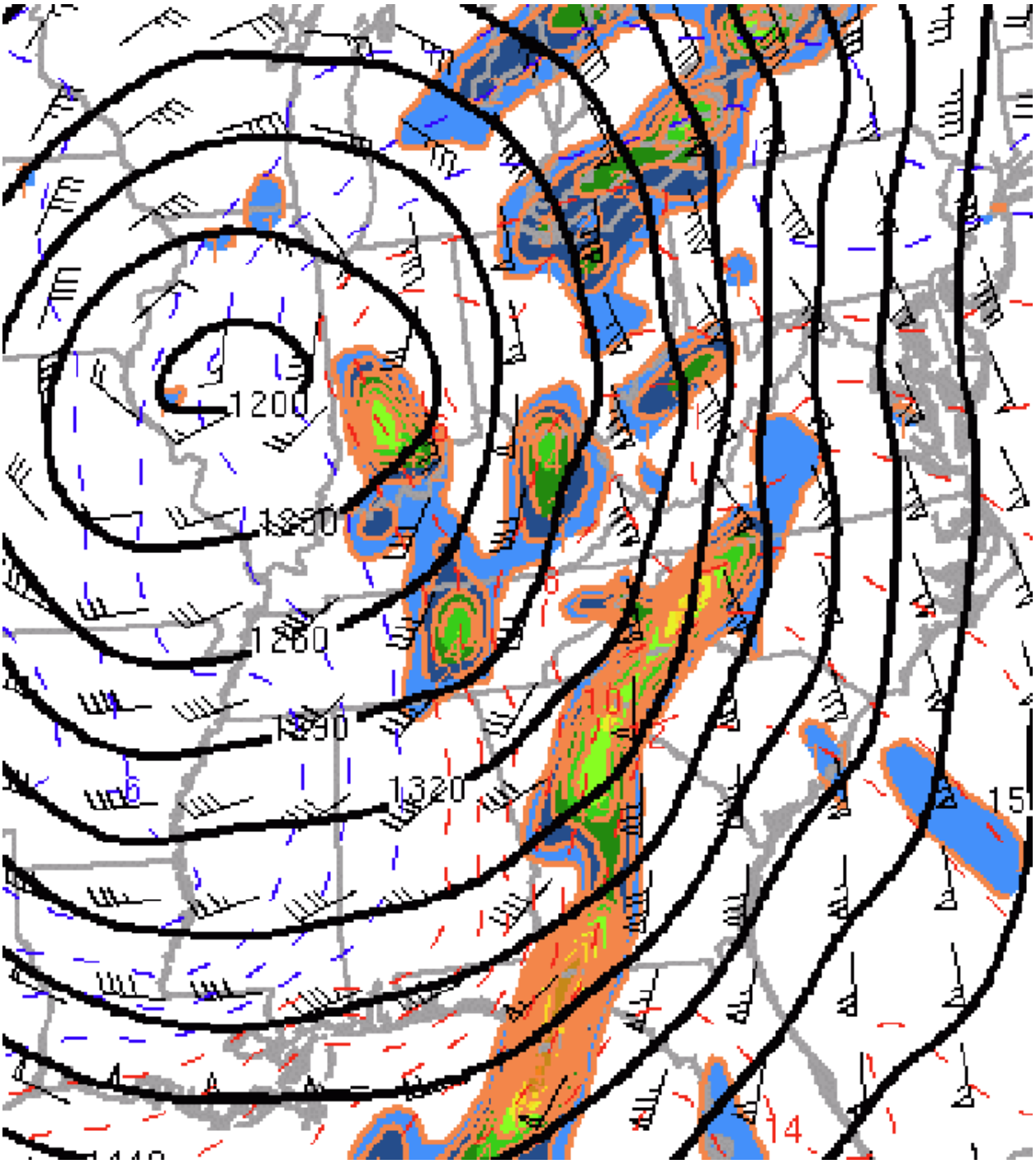


**Fig. 51.** 850 mb Petterssen frontogenesis (K (100 km)$^{-1}$ (3 hr)$^{-1}$; brown contours and color fill), wind (barbs), temperature (°C; dashed blue and red contours), and geopotential height (dam; black contours at 1700 UTC.